

Combined effect of nonmagnetic and magnetic scatterers on the critical temperatures of superconductors with different anisotropies of the gap

L. A. Openov^{a)}

Moscow State Engineering Physics Institute, 115409 Moscow, Russia

(Submitted 1 October 1997)

Pis'ma Zh. Éksp. Teor. Fiz. **66**, No. 10, 627–632 (25 November 1997)

The combined effect of nonmagnetic and magnetic defects and impurities on the critical temperatures of superconductors with different anisotropies of the gap is studied theoretically within the weak coupling limit of the BCS model. An expression is derived which relates the critical temperature to the relaxation rates of charge carriers on nonmagnetic and magnetic scatterers and to the coefficient of anisotropy of the superconducting order parameter on the Fermi surface. The particular cases of *d*-wave, (*s*+*d*)-wave, and anisotropic *s*-wave superconductors are briefly discussed. © 1997 American Institute of Physics. [S0021-3640(97)00122-9]

PACS numbers: 74.20.Fg, 74.62.Dh

This paper is motivated by the conflicting experimental results concerning the symmetry of the superconducting order parameter $\Delta(\mathbf{p})$ in high-temperature superconductors (HTSCs) and the depression of the critical temperature T_c of HTSCs by defects and impurities. Indeed, while the majority (though not all) of experiments support the hypothesis of *d*-wave superconductivity in HTSCs,¹ the observed depression of T_c by impurities or radiation-induced defects² is more gradual than is predicted theoretically for *d*-wave superconductors.³

To resolve this contradiction, a number of suggestions have been made, including anisotropic *s*-wave symmetry of $\Delta(\mathbf{p})$ (Ref. 4), momentum dependence of the impurity scattering (Ref. 5), strong coupling effects resulting in crossover from Cooper pairs to local bosons (see Ref. 6, etc). Note, however, that theoretical analysis of the depression of T_c by defects and impurities is usually restricted to the specific case of a spin-independent scattering potential, i.e., to the case of nonmagnetic scatterers only. Meanwhile a lot of experiments give evidence for the presence of magnetic scatterers (along with nonmagnetic ones) in non-stoichiometric HTSCs, e.g., in oxygen-deficient, doped or irradiated samples.⁷

The goal of this paper is to work out a theoretical framework for description of the combined effect of nonmagnetic and magnetic scatterers on T_c of a superconductor with anisotropic $\Delta(\mathbf{p})$ (in what concerns an isotropic *s*-wave superconductor, its T_c is insensitive to nonmagnetic defects,⁸ while the depression of T_c by magnetic defects is given by the well-known Abrikosov–Gor'kov theory.⁹) We use the weak coupling limit of the BCS model for superconducting pairing and the Born approximation for impurity scat-

tering. In what follows, we do not specify the microscopic mechanism of superconductivity. We set $\hbar = k_B = 1$ throughout the paper.

The Hamiltonian of a superconductor containing both nonmagnetic and magnetic scatterers reads

$$\begin{aligned} \hat{H} = & \sum_{\mathbf{p}, \sigma} \xi(\mathbf{p}) \hat{a}_{\mathbf{p}\sigma}^+ \hat{a}_{\mathbf{p}\sigma} + \sum_{\mathbf{p}, \mathbf{p}', \sigma, \sigma'} U(\mathbf{p}, \sigma; \mathbf{p}', \sigma') \hat{a}_{\mathbf{p}\sigma}^+ \hat{a}_{\mathbf{p}'\sigma'} \\ & + \sum_{\mathbf{p}, \mathbf{p}'} V(\mathbf{p}, \mathbf{p}') \hat{a}_{\mathbf{p}\uparrow}^+ \hat{a}_{-\mathbf{p}\downarrow}^+ \hat{a}_{-\mathbf{p}'\downarrow} \hat{a}_{\mathbf{p}'\uparrow}, \end{aligned} \quad (1)$$

where $\xi(\mathbf{p}) = \epsilon(\mathbf{p}) - \mu$ is the quasiparticle energy measured from the chemical potential, $U(\mathbf{p}, \sigma; \mathbf{p}', \sigma')$ is the matrix element for electron scattering by randomly distributed impurities (defects) from the state (\mathbf{p}', σ') to the state (\mathbf{p}, σ) , and $V(\mathbf{p}, \mathbf{p}')$ is the BCS pair potential.

We assume for simplicity that electron scattering is isotropic in momentum space, the amplitude for scattering by an isolated nonmagnetic (magnetic) scatterer being u_n (u_m). Then the relaxation times τ_n and τ_m are given by the standard ‘‘golden rule’’ formulas

$$\frac{1}{\tau_n} = 2\pi c_n |u_n|^2 N(0), \quad \frac{1}{\tau_m} = 2\pi c_m |u_m|^2 N(0), \quad (2)$$

where c_n and c_m are the concentrations of scatterers, $N(0)$ is the density of electron states at the Fermi level. Note that the commonly accepted expression for $|u_m|^2$ is $J^2 S(S+1)/4$, where J is the energy of electron-impurity exchange interaction, and S is the impurity spin.

In order to account for anisotropy of the superconducting state, we assume a factorizable pairing interaction of the form¹⁰

$$V(\mathbf{p}, \mathbf{p}') = -V_0 \phi(\mathbf{n}) \phi(\mathbf{n}'), \quad (3)$$

where $\mathbf{n} = \mathbf{p}/p$ is a unit vector along the momentum. Then the order parameter $\Delta(\mathbf{p})$ is¹⁰

$$\Delta(\mathbf{p}) = \Delta_0 \phi(\mathbf{n}), \quad (4)$$

where Δ_0 depends on the temperature. Thus the function $\phi(\mathbf{n})$ specifies the anisotropy of $\Delta(\mathbf{p})$ in momentum space ($\phi(\mathbf{n}) \equiv 1$ for isotropic pairing). A self-consistent equation for $\Delta(\mathbf{p})$ can be derived by a Green’s functions technique (see, e.g., Ref. 9). It is as follows:

$$\Delta(\mathbf{p}) = - \sum_{\mathbf{p}'} V(\mathbf{p}, \mathbf{p}') \langle \hat{a}_{-\mathbf{p}'\downarrow} \hat{a}_{\mathbf{p}'\uparrow} \rangle = -T \sum_{\omega} \sum_{\mathbf{p}'} V(\mathbf{p}, \mathbf{p}') \frac{\Delta_{\omega}(\mathbf{p}')}{\omega'^2 + \xi^2(\mathbf{p}') + |\Delta_{\omega}(\mathbf{p}')|^2}, \quad (5)$$

where $\omega = \pi T(2n+1)$ are Matsubara frequencies, and the equations for $\Delta_{\omega}(\mathbf{p})$ and ω' are

$$\Delta_{\omega}(\mathbf{p}) = \Delta(\mathbf{p}) + (c_n |u_n|^2 - c_m |u_m|^2) \sum_{\mathbf{p}'} \frac{\Delta_{\omega}(\mathbf{p}')}{\omega'^2 + \xi^2(\mathbf{p}') + |\Delta_{\omega}(\mathbf{p}')|^2}, \quad (6)$$

$$\omega' = \omega - i(c_n|u_n|^2 + c_m|u_m|^2) \sum_{\mathbf{p}'} \frac{i\omega' + \xi(\mathbf{p}')}{\omega'^2 + \xi^2(\mathbf{p}') + |\Delta_\omega(\mathbf{p}')|^2}. \quad (7)$$

Since $\Delta(\mathbf{p})=0$ at $T=T_c$, in the case $T \rightarrow T_c$ we have from (6), (7), taking (2) into account:

$$\Delta_\omega(\mathbf{p}) = \Delta(\mathbf{p}) + \frac{1}{2|\omega'|} (1/\tau_n - 1/\tau_m) \langle \Delta_\omega(\mathbf{p}) \rangle, \quad (8)$$

$$\omega' = \omega + \frac{1}{2} (1/\tau_n + 1/\tau_m) \text{sign}(\omega), \quad (9)$$

where the angle brackets $\langle \dots \rangle$ stand for an average over the Fermi surface (FS):

$$\langle \dots \rangle = \int_{\text{FS}} (\dots) \frac{d\Omega_{\mathbf{p}}}{|\partial\xi(\mathbf{p})/\partial\mathbf{p}|} \Big/ \int_{\text{FS}} \frac{d\Omega_{\mathbf{p}}}{|\partial\xi(\mathbf{p})/\partial\mathbf{p}|}. \quad (10)$$

Substituting (8) and (9) in (5) and taking (3) into account, we have after rather simple but time-consuming algebraic transformations:

$$\ln\left(\frac{T_{c0}}{T_c}\right) = \pi T_c \sum_{\omega} \frac{1}{|\omega| + \frac{1}{2}(1/\tau_n + 1/\tau_m)} \left[\frac{1}{2|\omega|} (1/\tau_n + 1/\tau_m) - \frac{\langle \phi(\mathbf{n}) \rangle^2}{\langle \phi^2(\mathbf{n}) \rangle} \frac{1/\tau_n - 1/\tau_m}{2(|\omega| + 1/\tau_m)} \right]. \quad (11)$$

Here T_{c0} is the critical temperature in the absence of impurities and defects (at $1/\tau_n = 1/\tau_m = 0$). At this stage it is convenient to introduce the anisotropy coefficient χ of the order parameter on the FS:^{10,4}

$$\chi = 1 - \frac{\langle \phi(\mathbf{n}) \rangle^2}{\langle \phi^2(\mathbf{n}) \rangle} = 1 - \frac{\langle \Delta(\mathbf{p}) \rangle^2}{\langle \Delta^2(\mathbf{p}) \rangle}. \quad (12)$$

For isotropic s -wave pairing we have $\Delta(\mathbf{p}) \equiv \text{const}$ on the FS; therefore, $\langle \Delta(\mathbf{p}) \rangle^2 = \langle \Delta^2(\mathbf{p}) \rangle$, and $\chi=0$. For a superconductor with d -wave pairing we have $\chi=1$, since $\langle \Delta(\mathbf{p}) \rangle=0$. The range $0 < \chi < 1$ corresponds to anisotropic s -wave pairing or to mixed ($d+s$)-wave pairing. The higher the anisotropy of $\Delta(\mathbf{p})$ (e.g., the greater the partial weight of a d -wave in the case of mixed pairing), the closer to unity is the value of χ .

Making use of the definition (12) and the formula¹¹

$$\sum_{k=0}^{\infty} \left(\frac{1}{k+x} - \frac{1}{k+y} \right) = \Psi(y) - \Psi(x), \quad (13)$$

where Ψ is the digamma function, we obtain from (11):

$$\ln\left(\frac{T_{c0}}{T_c}\right) = (1-\chi) \left[\Psi\left(\frac{1}{2} + \frac{1}{2\pi T_c \tau_m}\right) - \Psi\left(\frac{1}{2}\right) \right]$$

$$+ \chi \left[\Psi \left(\frac{1}{2} + \frac{1}{4\pi T_c} \left(\frac{1}{\tau_n} + \frac{1}{\tau_m} \right) \right) - \Psi \left(\frac{1}{2} \right) \right]. \quad (14)$$

In two particular cases of (i) both nonmagnetic and magnetic scattering in an isotropic s -wave superconductor ($\chi=0$) and (ii) nonmagnetic scattering only in a superconductor with arbitrary anisotropy of $\Delta(\mathbf{p})$ ($1/\tau_m=0$, $0 \leq \chi \leq 1$), Eq. (14) reduces to the well-known expressions^{9,10}

$$\ln \left(\frac{T_{c0}}{T_c} \right) = \Psi \left(\frac{1}{2} + \frac{1}{2\pi T_c \tau_m} \right) - \Psi \left(\frac{1}{2} \right) \quad (15)$$

and

$$\ln \left(\frac{T_{c0}}{T_c} \right) = \chi \left[\Psi \left(\frac{1}{2} + \frac{1}{4\pi T_c \tau_n} \right) - \Psi \left(\frac{1}{2} \right) \right], \quad (16)$$

respectively.

Equation (14) is obviously more general than Eqs. (15) and (16), which are commonly used for the analysis of experimental data on the depression of T_c by defects and impurities in HTSCs.¹² In fact, in making use of Eq. (15) or Eq. (16) one assumes *a priori* that either (i) the order parameter in HTSCs is isotropic in momentum space, or (ii) magnetic scatterers are completely absent in the HTSCs. The latter assumption is often supplemented with a speculation as to the pure d -wave symmetry of $\Delta(\mathbf{p})$ (Ref. 13; i.e., one intentionally restricts himself to the case $\chi=1$ instead of attempting to extract the value of χ from the experiment). In our opinion, the experimental dependence of T_c versus impurity (defect) concentration or radiation dose should be analyzed within the framework of the theory presented above; see Eq. (14). One should not guess as to the degree of anisotropy of $\Delta(\mathbf{p})$ and the type of scatterers, but try to *determine* the value of χ and relative weights of magnetic and nonmagnetic components in electron scattering through comparison of theoretical predictions with available or specially performed experiments.

Now let us consider the limiting cases of weak and strong scattering ($T_{c0} - T_c \ll T_{c0}$ and $T_c \rightarrow 0$ respectively). At $1/4\pi T_{c0} \tau_n \ll 1$ and $1/4\pi T_{c0} \tau_m \ll 1$ (weak scattering) one has from (14):

$$T_{c0} - T_c \approx \frac{\pi}{4} \left[\frac{\chi}{2\tau_n} + \frac{1-\chi/2}{\tau_m} \right]. \quad (17)$$

In the particular cases (i) and (ii) considered above, Eq. (17) reduces to the well-known expressions¹²

$$T_{c0} - T_c \approx \frac{\pi}{4\tau_m} \quad (18)$$

and

$$T_{c0} - T_c \approx \frac{\pi\chi}{8\tau_n} \quad (19)$$

for the depression of T_c from its initial value by magnetic (at $\chi=0$) or nonmagnetic (at arbitrary value of χ) scatterers respectively.

As to the strong scattering limit, we recall that in the BCS theory, nonmagnetic scattering alone is insufficient for the non- d -wave superconductivity ($0 \leq \chi < 1$) to be destroyed completely;¹⁰ at $1/\tau_m=0$, the value of T_c asymptotically goes to zero as $1/\tau_n$ increases (whereas T_c for a d -wave superconductor with $\chi=1$ vanishes at a critical value $1/\tau_n^c = \pi T_{c0}/\gamma \approx 1.764 T_{c0}$, with $\gamma = e^C \approx 1.781$, where C is the Euler constant). On the other hand, magnetic scattering in the absence of nonmagnetic scattering ($1/\tau_n=0$) is known to suppress the isotropic s -wave superconductivity with $\chi=0$ at a critical value $1/\tau_m^c = \pi T_{c0}/2\gamma \approx 0.882 T_{c0}$ (Ref. 9).

On the basis of Eq. (14) it is straightforward to derive the general condition for impurity (defect) depression of T_c for a superconductor having an arbitrary anisotropy coefficient χ and containing both nonmagnetic and magnetic scatterers:

$$\frac{1}{\tau_{\text{eff}}^c} = \frac{\pi}{\gamma} 2^{\chi-1} T_{c0}, \quad (20)$$

where τ_{eff}^c is the critical value of the effective relaxation time τ_{eff} , defined as

$$\frac{1}{\tau_{\text{eff}}} = \left(\frac{1}{\tau_m} \right)^{1-\chi} \left(\frac{1}{\tau_n} + \frac{1}{\tau_m} \right)^\chi. \quad (21)$$

From Eqs. (20) and (21) one can see that $1/\tau_{\text{eff}}^c$ increases monotonically with both $1/\tau_n$ and $1/\tau_m$ at any value of χ , with the exception of the case $\chi=0$, where $1/\tau_{\text{eff}}$ doesn't depend on $1/\tau_n$, see (21). If χ is close to unity (strongly anisotropic $\Delta(\mathbf{p})$), then $1/\tau_{\text{eff}} \approx 1/\tau_n + 1/\tau_m$, i.e., the contribution of nonmagnetic and magnetic scattering to pair breaking is about the same. If $\chi \ll 1$ (almost isotropic $\Delta(\mathbf{p})$), then $1/\tau_{\text{eff}} \approx 1/\tau_m$, i.e., τ_{eff} is determined primarily by magnetic scattering. The higher the anisotropy coefficient χ , the greater is the relative contribution of nonmagnetic scatterers to T_c depression as compared to magnetic scatterers. If nonmagnetic scattering is absent ($1/\tau_n=0$), then $1/\tau_{\text{eff}} = 1/\tau_m$ at any value of χ .

We note however that while the concept of the effective relaxation time τ_{eff} can be used for evaluation of the critical level of nonmagnetic and magnetic disorder, it is not possible to express T_c in terms of τ_{eff} in the whole range $0 \leq T_c \leq T_{c0}$; see Eq. (14). In other words, the combined effect of nonmagnetic and magnetic scattering on T_c cannot be described by a single universal parameter depending on the values of τ_n , τ_m , and χ . For example, for $1/\tau_m=0$ and $0 \leq \chi < 1$ one has $1/\tau_{\text{eff}}=0$ irrespective of the value of $1/\tau_n$. On the one hand, as follows from (20), the zero value of $1/\tau_{\text{eff}}^c$ in this case points to the fact that in a BCS superconductor with non- d -wave symmetry of $\Delta(\mathbf{p})$ the critical level of disorder cannot be reached in the absence of magnetic scattering, in accordance with Ref. 10. On the other hand, the zero value of $1/\tau_{\text{eff}}$ obviously doesn't imply that T_c of a not- d -wave superconductor is completely insensitive to nonmagnetic scatterers at $1/\tau_m=0$ and $0 < \chi < 1$; see Eq. (14). Hence, while the quantity $1/\tau_{\text{eff}}^c$ characterizes the critical strength of impurity (defect) scattering corresponding to $T_c=0$, the quantity $1/\tau_{\text{eff}}$ (when it is less than $1/\tau_{\text{eff}}^c$) doesn't determine the value of T_c unequivocally.

Based on Eqs. (20) and (21), it is possible to derive the following expression for the critical value of $1/\tau_n$ in the presence of magnetic scattering:

$$\frac{1}{\tau_n^c} = \frac{1}{\tau_m} \left[2 \left(\frac{\pi T_{c0} \tau_m}{2\gamma} \right)^{1/\chi} - 1 \right]. \quad (22)$$

This expression is valid as long as $1/\tau_m < \pi 2^{\chi-1} T_{c0} / \gamma$, since otherwise the superconductivity is completely suppressed solely by magnetic impurities. The value of $1/\tau_n^c$ decreases as $1/\tau_m$ increases at constant χ or as χ increases at constant $1/\tau_m$. The finite value of $1/\tau_n^c$ in the presence of magnetic scatterers could reconcile the experimentally observed² disorder-induced depression of T_c of HTSCs below 4.2 K with theories having other than purely d -wave symmetry of $\Delta(\mathbf{p})$ in HTSCs, e.g., anisotropic s -wave symmetry or mixed ($d+s$)-wave symmetry.

In conclusion, the results obtained provide a basis for evaluation of the degree of anisotropy of the superconducting order parameter (and hence its possible symmetry) as well as the type of scatterers (magnetic or nonmagnetic) in high- T_c superconductors through careful comparison of theoretical predictions with experiments on impurity-induced and radiation-induced lowering of the critical temperature. We hope that the present paper will serve as a stimulus for experiments on combined effect of nonmagnetic and magnetic scattering in the copper-oxide superconductors.

Note added in proof. After submission of this paper I became aware of a similar study by A. A. Golubov and I. I. Mazin [Phys. Rev. B **55**, 15146 (1997)], which generalizes the Abrikosov–Gor’kov solution to the case of a multiband superconductor with interband order parameter anisotropy.

This work was supported by the Russian Fund for Fundamental Research under Grant 97-02-16187. The author would like to thank V. F. Elesin and A. V. Krasheninnikov for fruitful discussions at the early stages of this work and V. A. Kashurnikov for helpful comments.

^{a)}e-mail: opn@supercon.mephi.ru

¹J. Annett, N. Goldenfeld, and A. J. Leggett, in *Physical Properties of High Temperature Superconductors*, Vol. 5, edited by D. M. Ginsberg, World Scientific, Singapore, 1996, and references therein.

²A. G. Sun, L. M. Paulius, D. A. Gajewski *et al.*, Phys. Rev. B **50**, 3266 (1994); J. Giapintzakis, D. M. Ginsberg, M. A. Kirk, and S. Ockers, Phys. Rev. B **50**, 15967 (1994); F. Rullier-Albenque, A. Legris, H. Berger, and L. Forro, Physica C **254**, 88 (1995); S. K. Tolpygo, J.-Y. Lin, M. Gurvitch *et al.*, Phys. Rev. B **53**, 12454 (1996); V. F. Elesin, K. E. Kon’kov, A. V. Krasheninnikov, and L. A. Openov, Zh. Eksp. Teor. Fiz. **110**, 731 (1996) [JETP **83**, 395 (1996)].

³R. J. Radtke, K. Levin, H.-B. Schüttler, and M. R. Norman, Phys. Rev. B **48**, 653 (1993); K. Levin, Y. Zha, R. J. Radtke *et al.*, J. Supercond. **7**, 563 (1994).

⁴L. A. Openov, V. F. Elesin, and A. V. Krasheninnikov, Physica C **257**, 53 (1996).

⁵G. Harań and A. D. S. Nagi, Phys. Rev. B **54**, 15463 (1996).

⁶M. V. Sadovskii and A. I. Posazhennikova, JETP Lett. **65**, 270 (1997).

⁷A. M. Finkel’shtein, V. E. Kataev, E. F. Kukovitskii, and G. B. Teitel’baum, Physica C **168**, 370 (1990); G. Xiao, M. Z. Cieplak, J. Q. Xiao, and C. L. Chien, Phys. Rev. B **42**, 8752 (1990); B. vom Hedt, W. Lisseck, K. Westerholt, and H. Bach, Phys. Rev. B **49**, 9898 (1994); J. Axnäs, W. Holm, Yu. Eltsev, and Ö. Rapp, Phys. Rev. B **53**, 3003 (1996); V. P. S. Awana, D. A. Landinez, J. M. Ferreira *et al.*, Mod. Phys. Lett. B **10**,

- 619 (1996); T. G. Togonidze, V. N. Kopylov, N. N. Kolesnikov, and I. F. Schegolev, *Czech. J. Phys.* **46**, 1379 (1996).
- ⁸P. W. Anderson, *J. Phys. Chem. Solids* **11**, 26 (1959).
- ⁹A. A. Abrikosov and L. P. Gor'kov, *Zh. Éksp. Teor. Fiz.* **39**, 1781 (1960) [*Sov. Phys. JETP* **12**, 1243 (1961)].
- ¹⁰A. A. Abrikosov, *Physica C* **214**, 107 (1993).
- ¹¹A. P. Prudnikov, Yu. A. Brychkov, and O. I. Marichev, *Integrals and Series* [in Russian], Nauka, Moscow, 1981, p. 655.
- ¹²P. S. Prabhu, M. S. R. Rao, U. V. Varadaraju, and G. V. S. Rao, *Phys. Rev. B* **50**, 6929 (1994); E. M. Jackson, B. D. Weaver, G. P. Summers *et al.*, *Phys. Rev. Lett.* **74**, 3033 (1995); S. K. Tolpygo, *Phys. Rev. Lett.* **75**, 3197 (1995); P. Monod, K. Maki, and F. Rullier-Albenque, *Phys. Rev. Lett.* **75**, 3198 (1995); T. Kluge, Y. Koike, A. Fujiwara *et al.*, *Phys. Rev. B* **52**, 727 (1995); M. Brinkmann, H. Bach, and K. Westerholt, *Phys. Rev. B* **54**, 6680 (1996); B. D. Weaver, G. P. Summers, R. L. Greene *et al.*, *Physica C* **261**, 229 (1996).
- ¹³J.-Y. Lin, H. D. Yang, S. K. Tolpygo, and M. Gurvitch, *Czech. J. Phys.* **46**, 1187 (1996); D. M. Ginsberg, J. Giapintzakis, and M. A. Kirk, *Czech. J. Phys.* **46**, 1203 (1996).

Published in English in the original Russian journal. Edited by Steve Torstveit.

Quasi-one-dimensional transport of nondegenerate electrons in two-dimensional systems with a fluctuation potential

B. A. Aronzon and E. Z. Meilikhov

Institute of Molecular Physics, Kurchatov Institute Russian National Science Center, 123182 Moscow, Russia

D. A. Bakaushin and A. S. Vedenev

Institute of Radio Engineering and Electronics, Russian Academy of Sciences, 141120 Fryazino, Moscow Region, Russia

V. V. Ryl'kov

Institute of Molecular Physics, Kurchatov Institute Russian National Science Center, 123182 Moscow, Russia; Institute of Radio Engineering and Electronics, Russian Academy of Sciences, 141120 Fryazino, Moscow Region, Russia

(Submitted 7 October 1997)

Pis'ma Zh. Éksp. Teor. Fiz. **66**, No. 10, 633–638 (25 November 1997)

A threshold vanishing of the Hall emf with decreasing gate voltage is observed at ≈ 77 K in semiconductor systems which are disordered as a result of a high built-in charge density near the plane of the 2D-electron channel. The effect is observed at a channel conductivity $\sigma \approx e^2/h$ and is due to a transition to nondegenerate-electron transport via a 2D percolation cluster having a quasi-1D character of the conduction. We have established that the conductance of “short” structures, having a length of the order of the correlation length of a percolation cluster, equals $\approx e^2/h$ per electron and is determined by isolated percolation paths having a lowered percolation threshold. These phenomena are a general property of disordered 2D systems. © 1997 American Institute of Physics. [S0021-3640(97)00222-3]

PACS numbers: 73.40.Qv, 73.61.–r

Metal–insulator–semiconductor structures with a high built-in charge density near the semiconductor–insulator interface are of interest in connection with the study of the electronic properties of disordered low-dimensional systems. Statistical fluctuations of the built-in charge density induce a chaotic potential relief on the semiconductor surface — a large-scale fluctuation potential (FP).¹ As a result of the strong scatter in the local quasi-2D electron density, the conductivity of the surface electron channel should be of a percolation character.² A characteristic feature of systems of this kind is that their conductivity is determined by the low fraction of charge carriers which are thermally activated to the percolation level. Here, in contrast to systems with a degenerate electron gas,³ the electron–electron interaction does not have a large effect on the conductivity nor on the localization of the charge carriers. On the contrary, most electrons are localized in the classical sense in the minima of the potential relief.⁴

We shall show that in the case of a strong FP and relatively high temperatures ($T \geq 77$ K) electron transport in 2D objects can be of a quantum quasi-1D character. The conductivity of samples which are wide and short (with a length comparable to the correlation length) is $\sim e^2/h$ per electron and is determined by a single percolation path with a lowered percolation threshold.

We took for the model objects structures with an inversion n channel on (100) p -Si and an insulator consisting of SiO_2 and Si_3N_4 layers 30 and 350 Å thick. Experiments were performed in the field-effect configuration at $T = 77 - 300$ K for different fixed values of the density n_t of the sources of the FP (traps on the SiO_2 - Si_3N_4 interface). The values of n_t were varied by electron injection.

The amplitude of the fluctuations of the surface potential is^{4,5} $\delta\phi_s = \Delta \ln^{1/2}(1 + R_s^2/r_0^2)$, where $\Delta = (e^2/\kappa)(\pi n_t)^{1/2}$ is the energy scale of the FP, R_s is the screening radius, r_0 is the distance between the plane of built-in charges and the 2D channel, e is the elementary charge, and κ is the dielectric constant. The strong-FP limit ($\Delta \gg kT$),⁴ i.e., where disorder radically changes the electronic properties of the system, obtains at densities $n_t \sim 10^{12} - 10^{13} \text{ cm}^{-2}$. Localized states are formed in the regions of the minima of the FP. The electrons that fill such states do not participate in conduction. However, they screen the components of the FP whose spatial scale is greater than the nonlinear-screening length $R_s = (n_t/\pi)/n_s$;⁴ here n_s is the total electron density (both localized and free electrons) in the channel, the free electron density being $n_c \ll n_s$. In other words, under the conditions of a strong FP electrons are predominantly localized and n_c is a power-law function of n_s : $n_c \propto n_s^{2\Delta/kT}$ (Ref. 4). Since the conductance G of the channel is proportional to n_c , we have $G \propto n_s^{2\Delta/kT}$. Therefore, if the relation between n_s and gate voltage V_g is known, then the degree of localization of the electrons can be analyzed on the basis of the dependence of G on V_g .

Figure 1 displays typical curves of the conductance $G(n_s)$ found from field-effect data for a structure with a gate of length $L = 140 \mu\text{m}$ and width $W = 20 \mu\text{m}$ for $n_t \approx 2 \times 10^{12} \text{ cm}^{-2}$ (the value $\Delta \approx 40 \text{ meV}$ at $T = 77 - 300$ K satisfied the strong-FP criterion). The dependence $n_s(V_g)$ was determined using the algorithm of Ref. 6. For weak inversion G varies with n_s according to a power law with exponent close to the computed value $2\Delta/kT$, in accordance with Ref. 4. In the case of strong inversion ($n_s \geq n_t$), as a result of screening of the FP $\delta\phi_s$ becomes $\sim kT$ and $G(n_s)$ becomes linear.

Thus, the structures demonstrate the classic dependence⁴ of $G(n_s)$ that is typical for the regime of nonlinear screening of the FP and which was observed, for example, in Ref. 6. Correspondingly, as V_g decreases, which is accompanied by an increase in the amplitude of the FP, a transition is expected from a slightly disordered effective 2D medium to a strongly disordered medium with percolation conductivity.^{2,7} It is believed that the transport coefficients (conductivity and Hall mobility μ_H) do not change much with such a transition.⁸ With respect to the Hall mobility this conclusion is confirmed by the fact that the Lorentz force acts on the free charge carriers, which determine the conductivity.

Meanwhile, Hall-effect experiments revealed interesting features. Figure 2 displays μ_H as a function of the channel conductivity σ . The curve was constructed from the experimental curves $G(V_g)$ and $\mu_H(V_g)$. The measurements were performed with different polarities of the magnetic field ($B = 1 \text{ T}$) using synchronous digital filtering.⁹ The

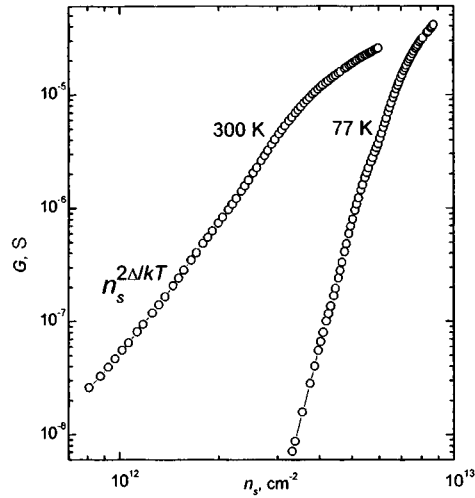


FIG. 1. Conductance G versus total electron density n_s in the inversion channel at 77 and 300 K for a structure with a large gate electrode.

threshold character of the dependence $\mu_H(\sigma)$ is noteworthy. As the gate voltage decreases, μ_H drops rapidly and reaches lower values than the minimum value determined by the criterion $l > \lambda$ (Ref. 1), where l and λ are, respectively, the mean free path length and the wavelength of the electrons. It is noteworthy that the “threshold” value of the conductivity (obtained by extrapolating the curve $\mu_H(\sigma)$ to the abscissa) agrees well with the value of e^2/h .

We note that features of this kind have also been observed previously (see Ref. 1). Investigations of inversion channels on a silicon surface at subhelium temperatures¹⁰ have revealed a group of samples, which have been termed *anomalous*, in which μ_H drops with decreasing T or V_g at $\sigma \sim e^2/h$. This result was interpreted in terms of a transition to electron transport along localized states below the mobility edge with con-

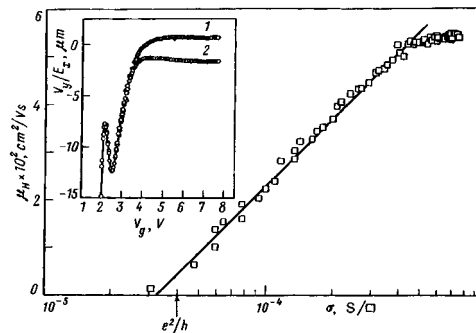


FIG. 2. Hall mobility versus channel conductivity at 77 K. Inset: V_y/E_x versus V_g with different polarities of the magnetic field. The divergence of curves 1 and 2 for $V_g \geq 3.5$ V is due to the appearance of the Hall effect.

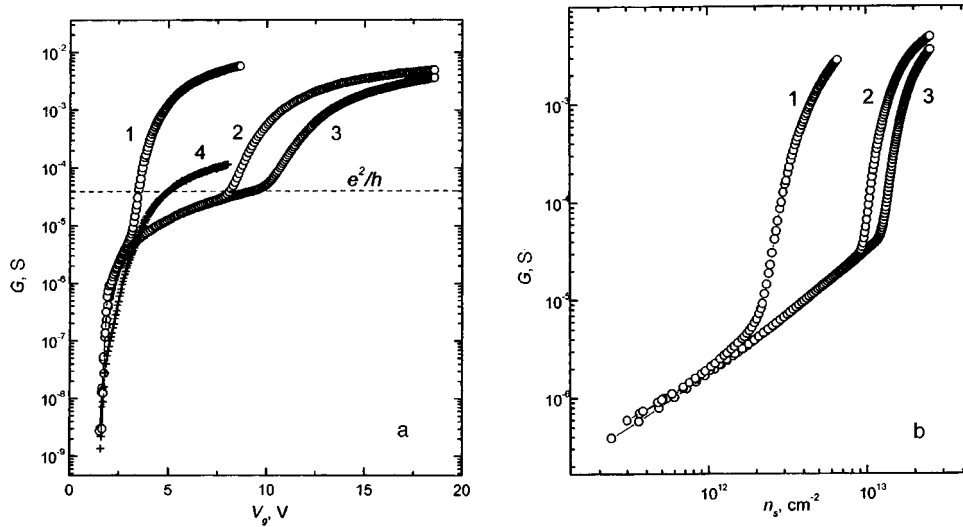


FIG. 3. a — Field-effect curves for a short-channel transistor with different values $n_i \approx 2.5 \times 10^{12}$ (1), 5.3×10^{12} (2), and $6.5 \times 10^{12} \text{ cm}^{-2}$ (3) and for a structure with a large gate with $n_i \approx 2 \times 10^{12}$ (4) at 77 K. b — G versus n_s for a short-channel transistor at 77 K.

ductivity not exceeding the minimum metallic conductivity.¹¹ In view of the smooth character of the FP and the quite high temperatures, transport along localized states under the conditions of our experiment is not significant.¹ On the contrary, we assume that in our situation the percolation character of the electron transport in a strong FP plays the determining role.

Experimental confirmation of the percolation character of conduction comes from observation of effects which are due to the existence of a macroscopic scale of self-averaging of the resistance. In disordered systems this scale is limited by the correlation length L_c , i.e., the characteristic size of the cells in a percolation cluster. According to percolation theory (see Ref. 7), L_c is determined by the product of the spatial scale of an inhomogeneity and a parameter that controls the variance of the local conductivity of the inhomogeneity. In our case $L_c \sim R_s(\delta\phi_s/kT)$, which can reach $\sim 1 \mu\text{m}$. For this reason, short samples — short-channel transistors with gate length $L = 5 \mu\text{m}$ comparable to L_c and width $W = 50 \mu\text{m}$ much greater than L_c — were taken as the objects of investigation.

The results of these experiments are presented in Fig. 3. As expected, for the case of percolation transport, here, in contrast to similar structures with “large” dimensions ($L, W \gg L_c$) studied above, the character of the field-effect curves is qualitatively different. The curves exhibit a kink, which does not occur in large samples, at values of the conductance G that approach e^2/h as n_i increases (compare curves 1–3 and 4 in Fig. 3a). In the region of weak inversion, where the effects of the FP are strongest and, according to Ref. 4, the conductivity varies with n_s according to a power law with exponent $2\Delta/kT \gg 1$ (see Fig. 1), the conductance $G(n_s)$ in short-channel structures is close to linear (Fig. 3b). On the basis of Ref. 4, this behavior of $G(n_s)$ should be attributed to the absence of electron localization despite the fact that the criterion of a strong FP is

satisfied ($\Delta \gg kT$). There is another noteworthy circumstance: In the region of weak inversion the function $G(V_g)$ does not depend on n_t ; this is not consistent with Ref. 4. This sharp change in the electronic properties of objects with decreasing channel length indicates that the conductivity under conditions of a strong FP is of a percolation character.

Proceeding now to a discussion of the results, let us examine the structure of a percolation cluster. As we have said, fluctuations of the built-in charge density induce, in a surface layer of the semiconductor, regions with a lowered potential, where, in the absence of degeneracy, the local conductivity is exponentially high (relative to the average value). These regions, which are coupled with one another by saddle regions (saddle points of the potential relief), form conducting chains whose length is of the order of the correlation length. These chains together form a percolation cluster. The saddle points lie in energy above the neighboring low-resistance regions which they connect and therefore their resistance is much higher than that of the latter. Considering the strong scatter in the saddle-point energies, we conclude that the resistance of a chain of length L_c and therefore of an arbitrary cell in a cluster is determined by a single saddle region — that with the highest resistance — lying in an interval $\sim kT$ near the percolation level.

The correlation function of the FP distinguishes, by its very nature, two limits of the spatial scales of the fluctuations: an upper limit (screening length R_s) and a lower limit (microscopic), controlled by the distance r_0 between the plane of built-in charges and the quasi-2D electron channel.⁴ We assume that the upper limit determines the size of the low-resistance regions with a lowered potential while the lower limit determines the size of the saddle regions. For our structures $r_0 \approx 30 \text{ \AA}$, which is comparable to the Bohr radius. Therefore the conductivity of the saddle regions is of a quantum one-dimensional character and equals e^2/h per electron.

Therefore the conduction mechanism under conditions of a strong FP is as follows. In large objects ($L, W \gg L_c$) the percolation level lies at the average position of the conduction band bottom on the semiconductor surface.⁴ The conductivity of the cells on a percolation structure is controlled by single saddle regions in an interval $\sim kT$ near the percolation level and is of a quantum nature. In other words, a cluster is a two-dimensional network whose resistance is determined by its quasi-1D sections. Under conditions of weak inversion the probability of finding an electron at the percolation level is determined by the energy gap ψ between the percolation level and the Fermi level. Therefore we have $\sigma \approx (e^2/h) \exp(-\psi/kT)$ for the conductivity of the sample as a whole. Since the main longitudinal voltage drop is across these high-resistance saddle regions, such a regime corresponds to a vanishingly weak Hall effect (Fig. 2). It is noteworthy that in the region where μ_H drops sharply regularly reproducible features appear in the dependence of the voltage V_y between the Hall probes (see inset in Fig. 2). According to our ideas,¹² these features are of a mesoscopic nature and are due to the restructuring of a percolation cluster, in the case at hand — as a result of the V_g dependence of the nonlinear-screening length of the FP. The amplitude δV_y of such fluctuations, relative to the longitudinal electric field E_x , gives an estimate of the correlation length $L_c \sim \delta V_y / E_x$ (Ref. 12). Under the experimental conditions (inset in Fig. 2) L_c equals several microns, which is equal in order of magnitude to the previously obtained estimate $L_c \sim R_s (\delta \phi_s / kT) \sim 1 \text{ \mu m}$.

The screening of the FP intensifies as V_g increases, and for $\delta\phi_s \sim kT$ the quantization condition breaks down in the saddle regions. As a result, the two-dimensional network of quasi-1D chains is modified into an effective 2D medium, and this is accompanied by the appearance of a Hall effect (Fig. 2). The channel conductivity corresponding to this transition should be of the order of e^2/h , since the system becomes two-dimensional and the network conductivity becomes e^2/h when the Fermi level and the percolation level cross.

A somewhat different situation is realized in short-channel structures. Here the conductivity of the system in the percolation limit is determined by percolation paths with anomalously low resistance. Effects of this kind have been studied for the example of hopping conduction.¹³ It appears that they play a determining role in our case as well. We assume that as a result of the relatively short length of the transistors ($L \sim L_c$) self-averaging of the conductivity, which occurs in systems with macroscopic dimensions, does not occur in them. At the same time, on account of the large width of the channel ($W \gg L_c$), a given statistical ensemble will realize most of its probabilistic states, including the appearance of the above-noted conducting chains with a low percolation level. Taking account of the strong scatter in the saddle-point energies, we arrive once again at the conclusion that the resistance of the system as a whole is determined by a small number of anomalously low-resistance percolation paths (in the limit, by one of them). In turn, the conductivity of the latter is determined by the highest-resistance saddle regions lying above the Fermi level (but substantially below the percolation level of large systems). Ultimately, the conductivity of the sample is determined by single saddle regions and equals $\sim e^2/h$ per electron. Taking account of the probability of a thermal transfer of an electron into a saddle region, we have $G \approx (e^2/h) \cdot \exp(-\psi/kT)$ for the conductance of the structure. This regime corresponds to the lower parts of curves 1–3 in Fig. 3a.

The lowering of the percolation level in “short” samples with respect to “large” samples results in a sharp increase in the fraction of free electrons at the expense of localized electrons. This is equivalent to weakening of the FP, which is apparently the reason why the $G(V_g)$ curves are observed to merge in the region of weak inversion (Fig. 3a). The decrease in the exponent of the dependence of G on n_s is probably also associated with this (compare Figs. 1 and 3b).

As V_g increases (and at the same time the energy gap ψ between the Fermi and percolation levels decreases), the conductance G increases, approaching the value e^2/h (Fig. 3a). As V_g increases further, the quasi-1D percolation system transforms into an effective 2D medium as a result of the intensified nonlinear screening of the FP. This process, which is accompanied by a sharp increase in the conductance, gives rise to a kink in the field-effect curves in the transition region, i.e., at $G \sim e^2/h$ (Fig. 3).

In conclusion, we note that the transition to the 1D conduction regime with a characteristic conductance e^2/h in structures with a length of the order of L_c , just as the vanishing of the Hall effect at $\sigma \sim e^2/h$ in “large” samples, is a general property of disordered 2D systems. We observed a kink in the curve $G(V_g)$ at $G \sim e^2/h$ in selectively doped GaAs–AlGaAs structures with a thin (30 Å) spacer and in GaAs transistors with a controlling Schottky barrier with a submicron-long channel.

We thank R. A. Suris and V. A. Gergel' for a lively discussion of the results. This work was supported by the Russian Fund for Fundamental Research (Grant No. 96-02-18429-a).

- ¹T. Ando, A. Fowler, and F. Stern, *Rev. Mod. Phys.* **54**, 437 (1982) [Russian transl., *Electronic Properties of Two-Dimensional Systems*, Mir, Moscow, 1985].
- ²J. W. Essam, *Rep. Prog. Phys.* **43**, 233 (1980).
- ³B. L. Altshuler and A. G. Aronov in *Electron-Electron Interaction in Disordered Systems*, edited by A. L. Efros and M. Pollak, North Holland, Amsterdam, 1985, p. 155.
- ⁴V. A. Gergel' and R. A. Suris, *Zh. Éksp. Teor. Fiz.* **84**, 719 (1983) [*Sov. Phys. JETP* **57**, 415 (1983)].
- ⁵J. R. Brews, *J. Appl. Phys.* **46**, 2181 (1974).
- ⁶A. S. Vedeneev, V. A. Gergel', A. G. Zhdan, and V. E. Sizov, *JETP Lett.* **58**, 375 (1993).
- ⁷B. I. Shklovskii and A. L. Efros, *Electronic Properties of Doped Semiconductors*, Springer-Verlag, New York, 1984 [Russian original, Nauka, Moscow, 1979].
- ⁸A. M. Dykhne, *Zh. Éksp. Teor. Fiz.* **59**, 110; 641 (1970) [*Sov. Phys. JETP* **32**, 63; 348 (1971)].
- ⁹A. S. Vedeneev, A. G. Zhdan, A. N. Ponomarev, and V. E. Sizov, *Prib. Tekh. Éksp.*, No. **4**, 132 (1994).
- ¹⁰E. Arnold, *Appl. Phys. Lett.* **25**, 705 (1974).
- ¹¹N. F. Mott and E. A. Davis, *Electronic Processes in Non-Crystalline Materials*, Clarendon, Oxford, Vol. 1, 22nd edition, 1979 [Russian translation, Mir, Moscow, 1982].
- ¹²B. A. Aronzon, A. S. Vedeneev, and V. V. Rylkov, *Physica A* (1997).
- ¹³A. I. Yakimov, N. P. Stepina, and A. V. Dvurechenskii, *Phys. Low-Dimens. Structures* **6**, 75 (1994).

Translated by M. E. Alferieff

Low-temperature motion of dislocations as a possible mechanism of formation of one-dimensional electronic structures in semiconductor crystals

N. I. Tarbaev,^{a)} G. A. Shepel'skiĭ, and E. A. Sal'kov

Institute of Semiconductor Physics, Ukrainian National Academy of Sciences, 252650 Kiev, Ukraine

(Submitted 14 July 1997; resubmitted 15 October 1997)

Pis'ma Zh. Éksp. Teor. Fiz. **66**, No. 10, 639–644 (25 November 1997)

A new mechanism is proposed for the formation of one-dimensional electronic structures in semiconductor crystals. The mechanism is based on controllable low-temperature glide of dislocations. Moving dislocations generate associations of intrinsic point defects in the form of one-dimensional chains, and the decay of the associations is impeded by low temperature. Experimental results and numerical estimates are presented for cadmium sulfide crystals. © 1997 American Institute of Physics. [S0021-3640(97)00322-8]

PACS numbers: 73.61.Ga, 61.72.-y

Linear defects in a crystal structure — dislocations — have generated special interest in recent years, since long rectilinear sections of dislocations can be regarded as one-dimensional ordered electronic systems in a semiconductor crystal lattice. In the present letter we examine a different, more obvious mechanism of formation of one-dimensional electronic structures in semiconductor crystals which is also associated with dislocations. The mechanism is based on the generation of chains of intrinsic point defects by moving dislocations.

As is well known, moving dislocations produce a large number of intrinsic point defects — vacancies and interstitial atoms — in a crystal. According to accepted ideas, dislocations generate defects in the form of associations of point defects. It can be assumed that the spatial distribution of such associations immediately after the passage of a dislocation will be ordered and will possess a definite periodic structure on account of the periodicity of the crystal itself. However, since the binding energy of such associations, as a rule, is low, they decay even at relatively low temperatures. The force fields around dislocations can only accelerate this decay. Therefore the spatial distribution of defects which are formed by moving dislocations is unstable. For this reason the low-temperature regime of dislocation motion in semiconductors is of special interest. Low-temperature plastic deformation (LTPD) gives an initial picture of defect formation by moving dislocations, since thermally activated mechanisms of interaction of defects are suppressed.

Our experimental investigations of LTPD in II–VI semiconductor compounds (CdS, CdTe, CdSe) showed that dislocation motion at low temperatures ($T=1.8-78$ K) does indeed give rise to characteristic features in the physical properties of the crystals that are

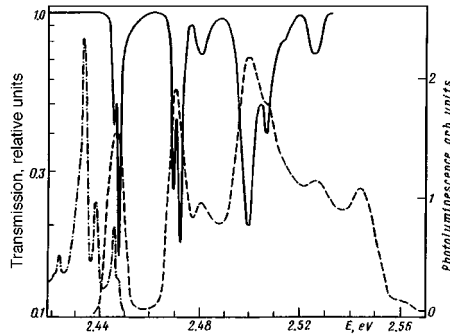


FIG. 1. Characteristic lines of the reduced optical transmission (solid curve), dislocation radiation (dot-dash curve), and excitation of DR (dashed line). $T=4.2$ K.

not observed for any other causes.¹ For example, special narrow, characteristic lines appear in the optical absorption (OA) and emission spectra. These lines have no analogs in the initial II–VI crystals and have not been previously observed. Furthermore, they do not appear even after plastic deformation at high temperatures ($T > 300$ K). Finally, these optical lines are not observed after intrinsic point defects are introduced into the crystal, for example, by irradiation with high-energy particles, even at low temperatures ($T < 78$ K). In the latter case, defects can be distributed uniformly over the volume but the distribution remains chaotic.

The results of an investigation of the OA and photoluminescence spectra obtained as a result of LTPD in cadmium sulfide crystals are presented in Fig. 1. They correspond to the deformation of the sample by uniaxial compression in the $\langle 11\bar{2}0 \rangle$ direction at $T=4.2$ K. The dislocation radiation (DR) at $T=4.2$ K consists of a series of characteristic emission bands, which we shall call dislocation bands. We shall examine the three strongest bands with energies 2.447, 2.440, and 2.435 eV. We note that the half-width of the dislocation bands in the temperature range 1.8–100 K is of the order of kT and is close to the half-width of the emission lines of bound excitons.

As one can see from the data in Fig. 1, the spectral positions of the optical transmission bands whence the OA coefficient was calculated completely coincide with the positions of the bands in the DR excitation spectrum. Such a detailed coincidence means that the OA and DR lines correspond to optical transitions between the electronic states of the same system of energy levels. The absorption coefficient α reaches 10^2 cm^{-1} even with a very low degree of LTPD ($\epsilon < 10^{-4}$).

Our data on optical absorption $\alpha(\nu)$ make it possible to estimate the average density N of optically active centers generated by LTPD from the well-known relation²

$$fN = \frac{ncm}{\pi e^2 \hbar} \int \alpha(\nu) d\nu, \quad (1)$$

where f is the oscillator strength, ν is the frequency, n is the index of refraction, c is the

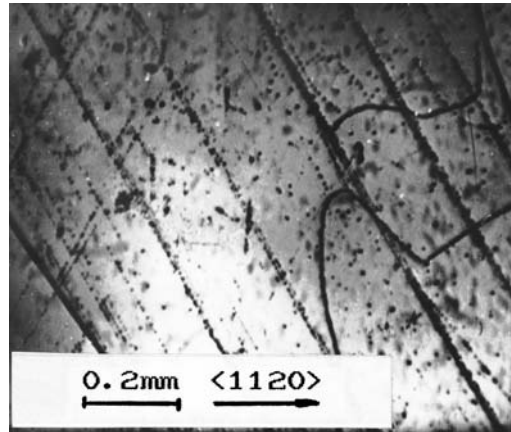


FIG. 2. LTPD-induced dislocation slip bands.

speed of light in vacuum, and e and m are the electron charge and mass, respectively. Substituting the numerical values of the quantities and the experimental values of α , we have

$$fN \approx 2 \times 10^{15} \text{ cm}^{-3}. \quad (2)$$

An estimate was made for the average density of dislocations, which are concentrated in slip bands, on the (0001) face of a crystal deformed at 77 K: $N_d = 10^5 \text{ cm}^{-2}$ (Fig. 2), which corresponded to absorption $\alpha = 10 \text{ cm}^{-1}$.

Here we must make an important remark concerning the nature of the LTPD-induced electronic states: The model of the electronic states directly of dislocation cores³ cannot satisfy this relation. Indeed, let us assume that these states refer directly to dislocation cores. The maximum density of states per unit length of a dislocation cannot exceed the number of atoms with disrupted coordination of the chemical bonds in the dislocation core, which is $\approx 10^7 \text{ cm}^{-1}$. Then, an oscillator strength $f \approx 10^3$ would be required to explain the strong optical absorption observed in our experiment. Such an oscillator strength is unrealistic and shows that the ‘‘core’’ model of DR and OA is invalid.

The degree of polarization of the OA and DR lines (intensity ratio for polarizations perpendicular and parallel to the C axis) is found to be low, falling in the range 1.1–1.3 for different samples. The real anisotropy is hidden primarily because of the experimentally established orientational degeneracy of the ‘‘dislocation’’ states.¹ Furthermore, allowance must be made for the strong depolarizing influence of the birefringence induced by the elastic stress fields near dislocations.

Narrow bands lying at the same energies as the OA peaks are also induced in the spectral distribution of the photoconductivity as a result of LTPD.

It is also important to note that all characteristic bands are strongly weakened or practically vanish completely after a crystal is held at room temperature even for 1 h.

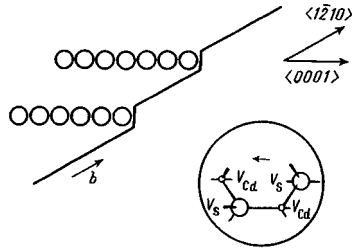


FIG. 3. Diagram illustrating the formation of one-dimensional chains of defects.

Therefore the low-temperature dislocation glide in a semiconductor gives rise to the formation of special unstable electronic states with very large oscillator strengths for optical transitions. It can be assumed that these states belong to some metastable associations of point defects arranged in an ordered fashion.

We shall examine the most likely model describing the formation of point defects by moving dislocations. In Refs. 3 and 4 it was established that the screw component dominates in dislocations in CdS which glide along a prismatic system. The mechanism leading to the formation of point defects during the motion of screw dislocations with steps is known.⁵ During deformation the steps engender either interstitial atoms or vacancies. For definiteness, let us examine the vacancy case. A moving step forms a continuous chain of defects. As a result, there arise chains of vacancies of the type $V_{Cd}-V_S-V_{Cd}-V_S-\dots$ and so on, which form one-dimensional structures oriented along the C axis. Two pairs of vacancies will be formed in each elementary event of climbing of a single 60- or 30-degree step.

The mechanism leading to the formation of chains of associations of intrinsic point defects by moving screw dislocations with steps is shown schematically in Fig. 3. The structure of an association (the period of a chain) is shown only on the enlarged fragment. We denote by N_j the average linear density of steps along screw segments. Our metallographic investigations show that under LTPD conditions the slip bands cross the entire sample with an approximately uniform emergence distribution of dislocations (etch pits) along the length of a slip band, so that the average travel distance of a dislocation equals 0.5 times the length of the slip band (Fig. 2). This also agrees with the quite high velocity of screw dislocations in CdS, which at 77 K can reach 5×10^{-2} cm/s.³ Hence the contribution of each step on a dislocation traversing an average path length to the average volume density of defects will equal 0.5×10^7 . Therefore the average volume density N of defects assembled into a chain can be calculated as

$$N \approx 0.5 N_d N_j \times 10^7 \text{ cm}^{-3}. \quad (3)$$

The density taken from Eq. (3) must be equated to the value of N obtained from OA (2): $N = 2 \times 10^{15}/f \text{ cm}^{-3}$. Substituting the experimental value $N_d = 10^5 \text{ cm}^{-2}$, we obtain a relation between N_j and f :

$$N_j \approx (1/f) \cdot 2 \times 10^2 \text{ cm}^{-1}. \quad (4)$$

Let us estimate N_j on the basis of expression (4), making reasonable assumptions about the oscillator strength f . As is well known, the maximum values of f correspond to bound-exciton states and range from 1 to 10 for II–VI crystals.⁶ In view of the strong localization of the excitons, we must choose the lower limit of this range: $f=1$. Hence we obtain $N_j=2\times 10^2\text{ cm}^{-1}$. This is a lower bound on N_j .

At the same time, an upper bound on N_j can be estimated independently. In Ref. 7 the stress t_d of dislocation stopping by single steps is related with N_j and the energy of formation W of point defects by the relation $t_d=N_jW/b^2$, where \mathbf{b} is the Burgers vector. Let us estimate the value of N_j for which control of the plastic flow of a crystal by the glide of screw dislocations with steps first appears. We take for t_d the experimentally obtained average threshold stress t_{thr} of plastic deformation for $T=77\text{ K}$. Allowing for the inclination of the glide plane with respect to the compression axis (60°), $t_d=0.5\text{ kbar}$. For W we take the total formation energy of two pairs of isolated vacancies:⁸ $W=2(W_{\text{VCd}}+W_{\text{VS}})-2(3.5+2)\text{ eV}=11\text{ eV}$. For CdS $b=0.414\times 10^{-7}\text{ cm}$. We obtain $N_j=t_db^2/W=5\times 10^3\text{ cm}^{-1}$. This is an upper bound on N_j . Using this value of N_j in Eq. (4) one can obtain a minimum value of the oscillator strength: $f\approx 0.1$.

Thus N_j lies in the range $2\times 10^2\text{--}5\times 10^3\text{ cm}^{-1}$. Hence it follows that the average volume density of point defects in chains falls in the range $2\times 10^{15}\text{--}5\times 10^{16}\text{ cm}^{-3}$ for the indicated value of α , which value seems entirely plausible.

We propose on the basis of the experimental results and estimates presented above the following model of electronic transitions that explains all features of the absorption and emission spectra of cadmium sulfide crystals subjected to LTPD. The transition responsible for the longest-wavelength optical absorption band and the DR band resonant with it corresponds to the excitation of excitons bound on a quasi-one-dimensional vacancy structure. The excitonic level is broadened into a band as a result of the overlapping of the wave functions of neighboring excitonic states along the chain. The remaining OA bands are due to transitions to excited states of the same system. In the latter case the excitation rapidly relaxes to the ground state and is not manifested in emission. Therefore large oscillator strengths f are explained by intrachain resonance interaction. Here there is an apt analogy with molecular crystals in which the molecules are arranged in one-dimensional oriented chains. The matrix element of the intrachain interaction in such crystals is at least two orders of magnitude larger than the matrix element of the interchain interaction.⁹

Important additional experimental facts also support the existence of one-dimensional structures and the narrow free-energy bands associated with them. For example, LTPD induces an appreciable anisotropy in the value of the photocurrent with respect to the orientation of the chains: The ratio I_{\parallel}/I_{\perp} reaches values of the order of 10. Furthermore, the current-carrier mobility estimated from photoconductivity measurements in OA dislocation bands is $\sim 5\times 10^5\text{ cm}^2/\text{V}\cdot\text{s}$. This is at least an order of magnitude higher than the mobility of electrons in the conduction band of cadmium sulfide.

This work was supported by the Fund for Basic Research of the Ukrainian Ministry of Science.

^{a)}e-mail: class@class.semicond.kiev.ua

-
- ¹N. I. Tarbaev, J. Schreiber, and G. A. Shepwlskii, *Phys. Status Solidi A* **110**, 97 (1988).
²A. M. Stoneham, *Theory of Defects in Solids*, Clarendon Press, Oxford, 1975 [Russian translation, Mir, Moscow, 1978, Vol. 1].
³V. D. Negry, Yu. A. Osipyanyan, and N. V. Lomak, *Phys. Status Solidi A* **126**, 49 (1991).
⁴Yu. Osipyanyan, V. F. Petrenko, G. K. Strukov, and I. I. Khodos, *Phys. Status Solidi A* **57**, 477 (1980).
⁵J. Hirth and J. Lothe, *Theory of Dislocations*, Wiley, New York, 1982, 2nd edition [Russian translation, Atomizdat, Moscow, 1972].
⁶D. G. Thomas and J. J. Hopfield, *Phys. Rev.* **175**, 1021 (1968).
⁷W. G. Jonson and J. J. Gilman, *J. Appl. Phys.* **31**, 632 (1960).
⁸T. Taguchi and B. Ray, *Prog. Cryst. Growth Character* **6**, 103 (1983).
⁹E. I. Rashba and M. D. Sturge (eds.), *Excitons*, North-Holland, Amsterdam, 1982 [Russian translation, Nauka, Moscow, 1985], Chap. 15.

Translated by M. E. Alferieff

Jahn–Teller effect on Sm^{3+} ions in fluctuating-valence compounds

T. S. Al'tshuler^{a)}

E. K. Zavoiskii Physicotechnical Institute, Russian Academy of Sciences, 420029 Kazan, Russia

M. S. Bresler

A. F. Ioffe Physicotechnical Institute, Russian Academy of Sciences, 194021 St. Petersburg, Russia

(Submitted 16 October 1997)

Pis'ma Zh. Éksp. Teor. Fiz. **66**, No. 10, 645–648 (25 November 1997)

The dynamic and static Jahn–Teller effects are observed in ESR on rare-earth ions, specifically, on Sm^{3+} ions in the fluctuating-valence material SmB_6 . © 1997 American Institute of Physics. [S0021-3640(97)00422-2]

PACS numbers: 71.70.Ej, 76.30.Kg

It is well known that the Jahn–Teller effect is ordinarily not observed by ESR on rare-earth ions.¹ The strong spin–orbit coupling that is characteristic for rare earths stabilizes the high-symmetry state and impedes the appearance of the Jahn–Teller effect. Apparently, the only exception thus far has been ESR on Er^{3+} ions in samarium hexaboride SmB_6 , where a dynamic Jahn–Teller effect has been observed.² This letter reports the observation of both dynamic and static Jahn–Teller effects, with the static effect being observed on rare earths.

We performed ESR studies on pure and doped (0.01 at. % europium) SmB_6 single crystals. The single crystals were grown from the fluxed melt and had dimensions $2 \times 1 \times 0.1$ mm. The measurements were made in the temperature interval 1.6–4.2 K with a Varian radio spectrometer at a frequency of 9.338 MHz. Samarium hexaboride (SmB_6) is a classic object in the physics of materials with fluctuating valence. The valence of samarium ions fluctuates with a frequency of 10^{13} – 10^{14} Hz between the states Sm^{2+} and Sm^{3+} (Ref. 3). Since the frequency of the ESR spectrometer is much lower (10^{10} Hz), it is impossible to observe signals on fluctuating ions. However, impurities and defects stabilize the valence of some of the samarium ions in the paramagnetic state Sm^{3+} (Ref. 4).

Completely identical ESR spectra from Sm^{3+} were observed on both samples at $T=1.6$ K in high fields (8–16 kOe) (Fig. 1). Apparently, pure SmB_6 contains defects which stabilize some of the ions in the Sm^{3+} state. Moreover, signals from Eu^{2+} , whose angular dependence is described well by a spin Hamiltonian with cubic symmetry, are also seen in europium-doped SmB_6 . The angular dependence of the ESR spectrum from Sm^{3+} ions at 1.6 K is presented in Fig. 2. The measurements were performed in the [100] plane; θ is the angle between the direction of the magnetic field and the (001) axis. The experimental data can be described on the basis of the assumption that there are two types

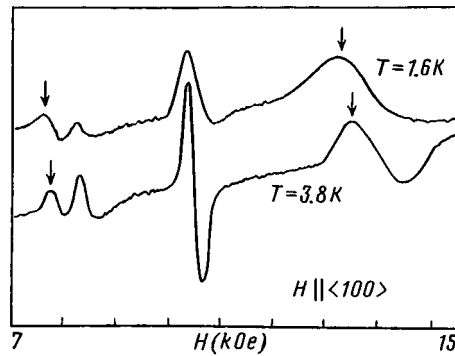


FIG. 1. Examples of traces of ESR signals from Sm^{3+} ions in SmB_6 at $\theta = 45^\circ$ and two temperatures: 1.6 K (curve 1) and 3.8 K (curve 2). The arrows mark the lines referring to a Γ_8 quartet; all other lines correspond to Γ_6 doublets.

of spectra. One spectrum is described by a quartet Γ_8 in a field with cubic symmetry and the other can be described by an axial (tetragonal) doublet. In accordance with the full cubic symmetry of the crystal, there are three types of doublets: Γ_{6x} , Γ_{6y} , and Γ_{6z} with

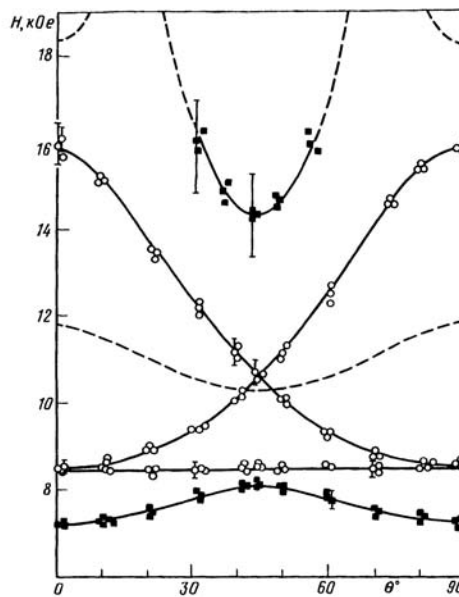


FIG. 2. Angular dependence of the positions of resonance lines accompanying rotation of the magnetic field in the $[100]$ plane. θ — angle between the direction of the magnetic field and the (001) axis. The filled squares correspond to the experimental position of the lines of the Γ_8 quartet and the unfilled circles correspond to Γ_{6x} , Γ_{6y} , and Γ_{6z} doublets. The solid lines describe the positions of the lines calculated theoretically using the parameter values of presented in the text. The dashed lines show the theoretical calculation for the lines of the Γ_8 quartet which are not observed experimentally.

distortions along the principal cubic axes. The parameters of these centers are determined from experiment: For the quartet $P=0.465$, $Q=-0.1$ and for the doublet $g_{\parallel}=2Q=0.42\pm 0.02$ and $g_{\perp}=(1/2)(3P-Q)=0.79\pm 0.02$. The observed values of P and Q are close to the theoretical values for the Sm^{3+} ion with spin $5/2$, $P_{\text{th}}=0.525$, viz., $Q_{\text{th}}=0.144$, i.e., the renormalization of these parameters, which is ordinarily due to the closeness of the $7/2$ level to the $5/2$ ground state, is not too large. One can see from Fig. 2 that the proposed values of the parameters describe well the angular dependence of the positions of the five observed lines for both samples. The calculations showed that the intensity ratios of the lines are also in agreement with experiment. It should be noted that the theory predicts four possible transitions for a quartet with effective spin $3/2$, while experimentally only two transitions are observed and all other transitions either lie in an experimentally inaccessible range of fields (above 16 kOe) or are partially or completely forbidden. Further analysis of the results showed that the state of the doublet is not independent, but rather it occurs as a result of the splitting of the quartet Γ_8 by a tetragonal field. As is well known,⁵ in this case the quartet Γ_8 splits into two doublets, one of which lies in the ground state with $g_{\parallel}=-0.2$ and $g_{\perp}=0.747$. These theoretically computed values of the g factors are close to the experimentally observed values. It is also necessary to take account of the fact that for such a splitting the factor g_{\parallel} is renormalized more strongly than g_{\perp} (Ref. 6). The splitting of a state of the quartet by a tetragonal field could be caused both by breaking of local symmetry (for example, presence of an impurity or defect near an ion with stabilized valence) and by the Jahn–Teller effect. We shall examine both possibilities.

1. The crystal structure of SmB_6 is identical to that of CsCl and consists of two interpenetrating cubic sublattices consisting of Sm ions and boron octahedra. The average valence of the fluctuating ions equals $+2.6$. In accordance with the principle of charge neutralization, there are $2.6/0.4 = 6.5$ Sm^{3+} ions for each vacancy in the samarium sublattice and 1.5 Sm ions for each Eu^{2+} impurity. If these Sm^{3+} ions are located next to a vacancy, then configurations with symmetry lower than tetragonal must exist. The absence of such centers in the experiment attests to the fact that the Sm^{3+} ions are grouped far from the vacancy whose charge they neutralize. At the same time, the Eu^{2+} ESR spectrum that we observed and the Er^{3+} spectrum in Ref. 2 indicate a cubic symmetry of the environment, i.e., the Sm^{3+} ions neutralizing the charge of Eu^{2+} and Er^{3+} are also located far from them.

2. In contrast to SmB_6 , compounds which are isostructural but possess integral valence [LaB_6 (Ref. 7), BaB_6 , YbB_6 (Ref. 1)] the standard (for Er^{3+} ions with $J=15/2$ in a cubic field) single ERS signal from a Γ_6 state is observed.⁸

3. As the temperature is increased to 4.2 K, the relative number of Γ_8 quartets increases and correspondingly the number of Γ_6 doublets of Sm^{3+} ions decreases. These facts are all easily explained by the Jahn–Teller effect and the much more complicated local breaking of the symmetry of the cubic field.

The Jahn–Teller effect in SmB_6 consists of spontaneous deformation of an octahedron, consisting of fluctuating Sm ions surrounding a paramagnetic impurity ion, along one of the principal cubic axes. This results in the splitting of the quartet state of the Sm^{3+} ion into two doublets. The states corresponding to deformations along the x , y , and z axes are degenerate. This is a static Jahn–Teller effect. As the temperature in-

creases, the vibrations of the metal ions near their new (shifted) positions of equilibrium intensify and the system consisting of a paramagnetic ion and its deformed environment starts to tunnel between the states corresponding to deformations along different cubic axes. The number of doublets decreases and correspondingly the number of Γ_8 quartets increases; this is due to a transition from the static to the dynamic Jahn–Teller effect.

The theory of the Jahn–Teller effect on Er^{3+} ions in samarium hexaboride can be used to describe the experimental results.^{1,9} In our case, the renormalization of the parameters P and Q as a result of a transition from the static to the dynamic Jahn–Teller effect is described by only one constant $c = c_1 + 4c_2$, where c_1 and c_2 are the matrix elements of transitions between different vibronic states. To describe our experimental results we must set $c = 0.905$ (for comparison, in the case of a purely static Jahn–Teller effect $c_1 = 1$ and $c_2 = 0$; in the case of the dynamic effect on Er^{3+} ions $c_1 = 0.7$ and $c_2 = 0.08$). Assuming that the transition from doublets to quartets with increasing temperature is due to a transition from the static to the dynamic Jahn–Teller effect, let us estimate the energy splitting of the quartet and doublet states according to the formula for the intensity ratio of the corresponding ESR lines:

$$\frac{I_4}{I_2} = \frac{N_4 \exp(-\Delta/T)w_4}{N_2w_2},$$

where I_4 and I_2 are quartet and doublet line intensities (taken from experiment for the strongest lines), N_4 and N_2 are the statistical weights of the quartet and doublet states, and w_4 and w_2 are the probabilities of the corresponding transitions. Taking the ratio w_4/w_2 from theory, we obtain $\Delta \cong 2.8$ K and $N_4/N_2 \cong 4.4$ for the europium-doped SmB_6 sample and $\Delta \cong 1.8$ K and $N_4/N_2 \cong 7.6$ for the pure SmB_6 sample. One can see that, to within the accuracy with which we can estimate in practice the desired quantities with a large width of the resonance lines, they are identical for both samples, which once again attests to the Jahn–Teller effect as being responsible for the observed phenomena: For the case of local symmetry breaking there should be no special correlation between the results for these quantities. The energy Δ characterizes in order of magnitude the barrier separating the vibronic states responsible for deformations of the octahedral environment of the Sm^{3+} ion with axes directed along different cubic axes. Therefore the observation of a center of only one type, which at low temperatures is in the doublet state and at higher temperatures transforms into a quartet, in the ESR spectrum allows us to conclude that both the static and dynamic Jahn–Teller effects were observed for rare-earth ions on Sm^{3+} centers in the compound SmB_6 . It was noted even back in Ref. 2 that the dynamic Jahn–Teller effect on Er^{3+} ions had been observed only in a compound with fluctuating valence (SmB_6) but it was not observed in compounds with integral valence — LaB_6 , BaB_6 , YbB_6 , CaB_6 , and others. Apparently, this is by no means accidental: It can be inferred that a strong electron–phonon interaction, which is responsible for the Jahn–Teller effect in samarium hexaboride, plays a large role in the nature of the fluctuating valence.

This work was supported by the Russian Fund for Fundamental Research (Grant 97-02-16235).

^{a)}e-mail: tatiana@dionis.kfti.kcn.ru

-
- ¹S. A. Al'tshuler and B. M. Kozyrev, *Electron Paramagnetic Resonance*, Academic Press, 1964 [Russian original, Nauka, Moscow, 1972].
- ²H. Sturm, B. Elschner, and K. H. Hoeck, *Phys. Rev. Lett.* **54**, 1291 (1985).
- ³T. Uemura, Y. Chiba, S. Kunii *et al.*, *J. Phys. Soc. Jpn.* **55**, 43 (1986).
- ⁴M. Kasaya, H. Kimura, Y. Isikawa *et al.*, *Valence Fluctuations in Solids*, North-Holland, Amsterdam, 1981, p. 251.
- ⁵A. Abragam and B. Bleaney, *Electron Paramagnetic Resonance of Transitions Ions*, Clarendon Press, Oxford, 1970 [Russian translation, Mir, Moscow, 1973], Chapter 18.
- ⁶A. A. Antipi, I. N. Kurkin, L. Z. Potvorova, and L. Ya. Shekun, *Fiz. Tverd. Tela (Leningrad)* **7**, 3209 (1965) [*Sov. Phys. Solid State* **7**, 2596 (1965)].
- ⁷H. Luft, K. Baberschke, and K. Winzer, *Phys. Lett. A* **95**, 186 (1983).
- ⁸K. R. Lea, M. J. M. Leask, and W. P. Wolf, *J. Phys. Chem. Solids* **23**, 1381 (1962).
- ⁹H. Sturm, Dissertation, Darmstadt, 1985.

Translated by M. E. Alferieff

New model for systems of mesoscopic Josephson junctions

A. I. Belousov and Yu. E. Lozovik^{a)}

Institute of Spectroscopy, Russian Academy of Sciences, 142092 Troitsk, Moscow Region, Russia

(Submitted 20 October 1997)

Pis'ma Zh. Éksp. Teor. Fiz. **66**, No. 10, 649–654 (25 November 1997)

Quantum fluctuations of the phases of the order parameter in two-dimensional arrays of mesoscopic Josephson junctions and their effect on the destruction of superconductivity in the system are investigated by means of a quantum-cosine model that is free of the incorrect application of the phase operator. The proposed model employs trigonometric phase operators and makes it possible to study arrays of small superconducting granules, pores containing superfluid helium, or Josephson junctions in which the average number of particles n_0 (effective bosons, He atoms, and so on) is small, and the standard approach employing the phase operator and the particle number operator as conjugate operators is inapplicable. There is a large difference in the phase diagrams between arrays of macroscopic and mesoscopic objects for $n_0 < 5$ and $U < J$ (U is the characteristic interaction energy of the particles per granule and J is the Josephson coupling constant). Re-entrant superconductivity phenomena are discussed. © 1997 American Institute of Physics. [S0021-3640(97)00522-7]

PACS numbers: 73.23.Ps, 74.50.+r, 74.20.Mn

The development of microlithographic methods has now made it possible to produce regular arrays of extremely small metallic granules, Josephson junctions, and so on. The study of the properties of such objects is of interest not only from the fundamental standpoint but also in connection with their possible application in nanoelectronics. For this reason, a great deal of attention is now being devoted to the investigation of models reflecting the main properties of mesoscopic Josephson arrays (see Refs. 1–9 and the literature cited therein).

In the present letter we call a granule (or a pore containing superfluid He) *mesoscopic* if the rms fluctuations of the number of effective bosons, viz., “Cooper pairs” (or He atoms in a pore), are comparable to the average number of particles. We do not address the question of the character of the transition of an individual granule to the superconducting state (or helium in a pore to the superfluid state), making the assumption that this transition (or crossover) has already occurred at a higher temperature T_{c_0} and that the concept, which we employ below, of an effective boson (particle) is defined. In this connection we note only that, just as for nucleon pairing in nuclei, strictly speaking, there does not exist a critical size of granules in which pairing is possible (but, for example, the parity of the number of electrons, the character of the filling of the levels,

and so on are important). The exposition below concerns an array of mesoscopic superconducting granules, but the analysis can obviously be extended to the case of superfluid helium in a porous medium.

In the present letter we show that the application of the phase and particle number operators as conjugate variables¹ ordinarily employed for describing such systems (in a quantum *XY* model) is limited to systems of *macroscopic* granules, while in the case of a small average number of particles per granule other models that do not employ the incorrect “phase operator” are required (see below). Recently, a boson Hubbard model^{7,8} that takes account of not only quantum fluctuations of the phases but also the modulus of the superconducting order parameter was used to investigate the superconducting properties of an array of mesoscopic granules. However, it is of interest to examine a system in which the fluctuations of the local superfluid density on the granules are small even in the mesoscopic region, and the quantum fluctuations of the phases of the order parameter play the main role in the destruction of the global superconducting state of the array.

At temperatures below the temperature T_{c_0} at which superconductivity is established in an individual granule the state of the system is determined by two parameters:^{8,10} a) the ratio of the characteristic Coulomb interaction energy of the particles $E_C \sim U/2$ in a granule with self-capacitance $C_0 = 4e^2/U$ (the mutual capacitances are assumed here to be much larger than C_0 and their contribution is neglected) and the Josephson tunneling energy for particles tunneling between granules $E_J \sim J$, the corresponding dimensionless quantum parameter being $q \equiv \sqrt{U/J}$, and b) the dimensionless temperature of the system $T \equiv k_b T/J$.

1. The superconducting properties of an array of “macroscopic” superconducting granules have traditionally been investigated in a quantum *XY* model with the Hamiltonian

$$\hat{H}_{XY} = J \sum_{\langle i,j \rangle} (1 - \cos(\hat{\varphi}_i - \hat{\varphi}_j)) + \frac{U}{2} \sum_i (\hat{n}_i - n_0)^2, \quad (1)$$

where the sum $\sum_{\langle i,j \rangle}$ in Eq. (1) extends over all nonrepeating pairs $\langle i,j \rangle$ of neighboring lattice sites. The phases of the order parameter $\varphi_i \in [0, 2\pi)$ and the particle number operator \hat{n}_i in the i th granule is assumed, starting with Anderson’s work,¹ to be conjugate to the “phase operator” $\hat{\varphi}_i$: $\hat{n}_i - n_0 = \tilde{j} \partial / \partial \varphi_i$. We note that the direct application of such a “phase operator” $\hat{\varphi}$ is, strictly speaking, incorrect, if for no other reason than that its effect is to transfer the state out of the domain of definition (the set of periodic functions $\psi(\varphi + 2\pi) = \psi(\varphi)$). Moreover, direct quantization of the order parameter as $\psi = \Delta e^{\tilde{j}\varphi} \rightarrow \hat{a} = \sqrt{\hat{n}} \hat{e}^{\tilde{j}\varphi}$ gives, in view of the boundedness of the spectrum of the particle number operator $\hat{n} = \hat{a}^\dagger \hat{a}$, a nonunitary operator $\hat{e}^{\tilde{j}\varphi}$. This makes it impossible to introduce a hermitian phase operator and leads to many paradoxes.¹¹

Many such difficulties can be circumvented by considering the “trigonometric” operators $\widehat{\cos} \varphi$ and $\widehat{\sin} \varphi$ (which do not commute with each other), while leaving the phase operator $\hat{\varphi}$ itself undefined.¹² In this approach, all operators of physical quantities which are periodic functions of the phase (in terms of the quantum *XY* model) must be rewritten as sums of trigonometric functions, followed by the substitutions

$$\begin{aligned}\cos(\varphi) \rightarrow \widehat{\cos} \varphi &= \frac{1}{2} \left(\hat{a}^\dagger \frac{1}{\sqrt{\hat{n}+1}} + \frac{1}{\sqrt{\hat{n}+1}} \hat{a} \right), \\ \sin(\varphi) \rightarrow \widehat{\sin} \varphi &= \frac{\tilde{J}}{2} \left(\hat{a}^\dagger \frac{1}{\sqrt{\hat{n}+1}} - \frac{1}{\sqrt{\hat{n}+1}} \hat{a} \right),\end{aligned}$$

where the operators \hat{a}^\dagger and \hat{a} are Bose particle creation and annihilation operators, and $\hat{n} = \hat{a}^\dagger \hat{a}$. As n_0 increases, when the rms fluctuations of the particle number in a granule are much smaller than their average value, the boundedness of the spectrum of the operator \hat{n} becomes unimportant and the “quantum trigonometric operators” $\widehat{\cos} \varphi$ and $\widehat{\sin} \varphi$ introduced above transform into their quasiclassical limit $\cos(\varphi)$ and $\sin(\varphi)$.

Applying the procedure described above to the Hamiltonian (1) of for our system we have

$$\hat{H} = J \sum_{\langle i,j \rangle} (1 - \widehat{\cos} \varphi_i \widehat{\cos} \varphi_j - \widehat{\sin} \varphi_i \widehat{\sin} \varphi_j) + \frac{U}{2} \sum_i (\hat{n}_i - n_0)^2. \quad (2)$$

In what follows we shall, for brevity, refer to the model (2) as the *quantum cosine model*.

In the present letter we are interested in the system (2) with *integral* occupation numbers, when the average number of bosons in each granule $n_0 = \langle a_i^\dagger a_i \rangle$ is an *integer*. It can be shown (see Ref. 5 for an analysis of this case in the boson Hubbard model) that under this condition and at $T=0$ the model (2) belongs to the same universality class as the quantum *XY* model (1). However, at *finite* temperatures the critical behavior of the quantum cosine model will be identical — in contrast to the system at zero temperature — to the critical behavior of the quantum *XY* model in some *finite* range of values of the average occupation number n_0 of the granules in the system (near integral values of n_0).

2. To calculate the properties of the system (2) in the plane of controlling parameters $\{q, T\}$, we used the quantum Monte Carlo method of integration along trajectories in a “checkerboard” modification,¹³ where the degrees of freedom of the discretized system are the occupation numbers $\{n_i^p\}$ of the sites of a three-dimensional lattice $N \times N \times 4P$ formed by $4P$ -fold multiplication of the initial $N \times N$ lattice along the imaginary-time axis.

In analyzing the superconducting properties of the array, attention was focused mainly on the analysis of the superfluid component fraction (the analog of the “helicity modulus” in the quantum *XY* model; see Ref. 14), the expression for which in terms of the quantum cosine model (2) has the form

$$\nu_s = - \frac{1}{N^2} \langle \hat{T}_x \rangle - \frac{1}{N^2 T P} \sum_{\tau=0}^{P-1} \langle \hat{j}_x^{(p)}(\tau) \hat{j}_x^{(p)}(0) \rangle, \quad (3)$$

$$\hat{T}_x = - \sum_i (\widehat{\cos} \varphi_{i+x} \widehat{\cos} \varphi_i + \widehat{\sin} \varphi_{i+x} \widehat{\sin} \varphi_i),$$

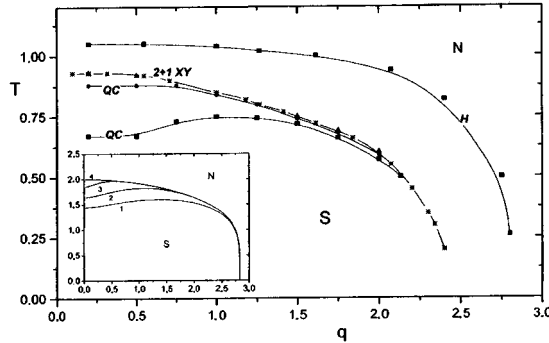


FIG. 1. Phase diagrams of the quantum cosine model (QC), the boson Hubbard model (H),⁸ and the quantum XY model (2+1 XY)¹⁷ (*S* — superconducting state, *N* — normal state). Inset: Computational results obtained in mean field theory:¹⁵ 1 — $n_0=1$; 2 — $n_0=2$; 3 — $n_0=6$; 4 — quantum XY model ($n_0=\infty$); here and below the symbols represent the quantum Monte Carlo results: unfilled symbols — $N=10$, filled symbols — $N=6$; squares — $n_0=1$, circles — $n_0=3$, triangles — $n_0=5$, rhombi — $n_0=7$, asterisks — quantum XY model.

$$\hat{J}_x^{(p)} = \sum_i (\widehat{\sin} \varphi_{i+x} \widehat{\cos} \varphi_i - \widehat{\cos} \varphi_{i+x} \widehat{\sin} \varphi_i), \quad \hat{J}_x^{(p)}(\tau) = e^{\tau \beta \hat{H}/P} \hat{J}_x^{(p)} e^{-\tau \beta \hat{H}/P}.$$

The superfluid component fraction was also found in terms of the fluctuations of the “winding number.”^{6,13}

An important quantity required for investigating the role of the mesoscopic nature of the system are the fluctuations of the particle number over the granules:

$$\delta n^2 = \frac{1}{4PN^2} \left\langle \sum_{p=0}^{4P-1} \sum_i (n_i^p - n_0)^2 \right\rangle. \quad (4)$$

3. Let us examine the Monte Carlo results for the quantum cosine model (2). The main quantity describing the state of the system at a given point $\{q, T\}$ of the phase diagram (Fig. 1) is the superfluid component fraction ν_s . Vanishing of ν_s indicates disordering of the system. The measured curves of the superfluid component fraction versus the temperature T for fixed values of the quantum parameter q are presented in Fig. 2. This figure shows the computational results for a $N \times N = 6 \times 6$ system with $n_0 = 1, 3, 5$, and 7 and, for comparison, for the quantum XY model (1) also. For a weak interparticle interaction in the granules $q < 1$ (which in terms of the XY model corresponds to a small role of quantum fluctuations of the phase of the order parameter) the superconductor–metal transition temperature T_c depends strongly on the average number of particles n_0 in a granule (see Fig. 2a). The temperature $T_c(q)$ can be estimated from the universal relation $\nu_s(q; T_c) = 2T_c/\pi$ (Ref. 14). It is evident from the figure that to suppress fluctuation phenomena in a system of mesoscopic granules or pores requires *lower* temperatures than in the case of systems of macroscopic granules. As the particle density increases (transition to the case of an array of macroscopic granules), for $n_0 > 5$ the plots of $\nu_s(T; n_0)|_{q=\text{const}}$ merge, to within the limits of the measurement error, and the model (2) goes over to its limit — the quantum XY model. This observation is also confirmed in Fig. 3, which displays the dependence of the superfluid component fraction

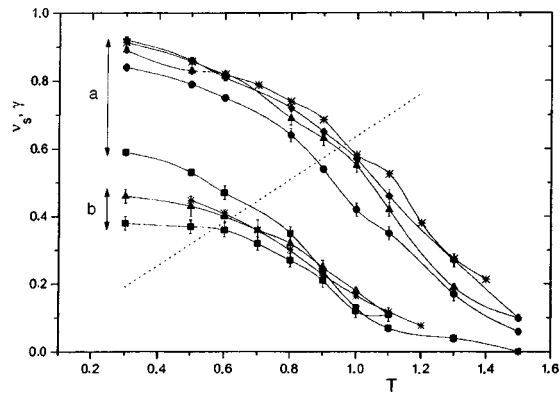


FIG. 2. Superfluid component fraction ν_s (helicity modulus γ in the case of the quantum XY model) versus temperature T : a) $q=0.2$; b) $q=2.0$; the dotted line shows the curve $2T/\pi$. A spline interpolation is drawn in as an aid to the eye. The statistical errors, which are not shown, are less than the size of the corresponding symbols.

in the models (2) and (1) on the quantum parameter q at $T=0.5$. We note that for $q>1$ the properties of the models under study differ very little, and therefore the effects of the mesoscopicity of the granules in the array are very small. This is confirmed in Figure 2b.

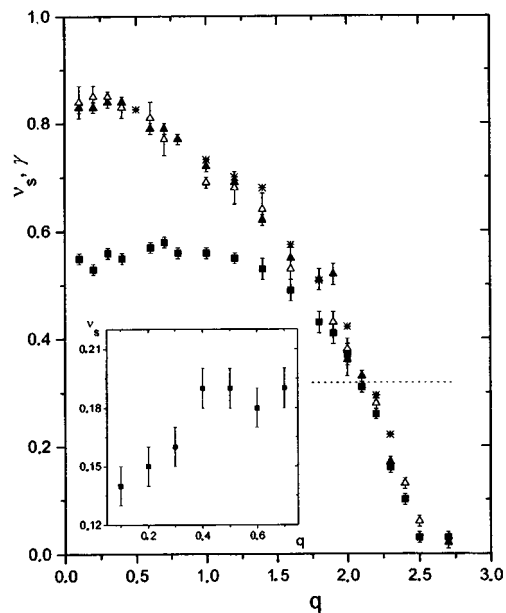


FIG. 3. Superfluid component fraction ν_s (helicity modulus γ in the case of the quantum XY model) versus the quantum parameter q at $T=0.5$; the dotted line shows the line $1/\pi$. Inset: $\nu_s(q)$ at $T=1$.

An interesting effect which we found in our calculations is *re-entrant superconductivity* of an array of mesoscopic granules with respect to the parameter q (determining the characteristic particle interaction energy). The *increase* in the density of the superfluid component with increasing quantum parameter q at a fixed temperature T , clearly seen in Fig. 3, is confirmed by the computational results for the model (2) in mean field theory¹⁵ (see Fig. 1).

The phase diagram of an ordered two-dimensional Josephson array of mesoscopic granules was constructed using the results presented above (see Fig. 1). For comparison, the computational result obtained in mean field theory, which is in qualitative agreement with the Monte Carlo data, is also shown. We note, for comparison, that taking the fluctuations of the modulus of the order parameter (local superfluid density) into account in the boson Hubbard model *increases* the superconducting transition temperature of a mesoscopic system.⁸

The character of the phase transition occurring along the line $T_c(q)$ can be analyzed in greater detail by analyzing the fluctuations of the particle number over the granules (4) as a function of the temperature and quantum parameter. The calculations show that as the temperature increases, the fluctuations of the particle number over the granules increases, as is characteristic for a transition to a state with a higher conductivity. Therefore, at finite temperatures the line of phase transitions $T_c(q)$ (see Fig. 1) is a line of superconductor-to-metal transitions (for $T < T_c(q)$). Conversely, at a fixed temperature the particle-number fluctuations $\delta n^2(q)$ as a function of the quantum parameter q decrease, as is characteristic for a (finite-temperature crossover) transition to a Mott insulator state.¹⁶

From the relative rms particle-number fluctuations $\epsilon_n \equiv \sqrt{\delta n^2/n_0^2}$ it can be concluded that the value $\epsilon = \epsilon_n^{\text{mes}} \sim 0.5$ can be regarded as a criterion for determining the mesoscopicity of granules in the array, namely, for smaller relative fluctuations the system can be viewed as consisting of macroscopic granules and can be described by the quantum XY model (1).

4. Thus, a new model has been proposed for systems of mesoscopic Josephson junctions — the quantum cosine model (2), which takes into account the quantum fluctuations of the phases of the order parameter and does *not* employ an incorrect definition of the “phase operator.” This model can be used to investigate the properties of systems of mesoscopic granules or pores containing a superfluid liquid, where the relative fluctuations of the number of “effective bosons” over the granules or atoms of the liquid in the pores are large and the quantum XY model (1) is inapplicable.

The computational results show that in the case of a system of weakly interacting particles (for $q < 1$) the temperature at which a global superconducting state appears depends strongly on the particle density, approaching *from below* the metal–superconductor transition temperature in a system of macroscopic granules or pores. It was found that the corresponding “macroscopic” limit, where the system is adequately described in a quantum XY model (1), is reached at comparatively low densities, $n_0 \sim 5$.

In the region of large quantum fluctuations of the phases ($q > 1$), the relative fluctuations of the particle number over the granules are strongly suppressed by the interac-

tion, and mesoscopic effects are important only at low temperatures ($T < 0.5$) and low densities ($n_0 \sim 1$).

As one can see from the computational results, the proposed quantum cosine model (2) does not (at least in the investigated range of the controlling parameters) exhibit re-entrant superconductivity with respect to *temperature*, where for some values of the quantum parameter q a global superconducting state is absent at both high and low temperatures. However, for a weak interparticle interaction, when $q < 1$, there is re-entrant superconductivity with respect to the *quantum parameter* q . We found that for the model (2), in contrast to the behavior of the Hubbard model and the quantum XY model, the degree of disorder in the system increases with decreasing interaction of the bosons (with decreasing force of quantum fluctuations of the phases in terms of the quantum XY model).

We thank V. F. Gantmakher for a helpful discussion of the results of this work. This work was supported by grants from the Russian Fund for Fundamental Research and the programs “Physics of Solid-State Nanostructures” and “Surface Atomic Structures.”

^{a)}e-mail: lozovik@isan.troitsk.ru

-
- ¹P. W. Anderson, in *Lectures in The Many Body Problem*, Vol. 2, edited by E. R. Caianiello, Academic Press, New York, 1964.
- ²J. B. Kim and M. Y. Choi, *Phys. Rev. B* **52**, 3624 (1997).
- ³V. F. Gantmakher, V. M. Teplinskiĭ, and V. N. Zverev, *JETP Lett.* **62**, 887 (1995).
- ⁴P. Lafarge, M. Matters, and J. E. Mooij, *Phys. Rev. B* **54**, 7380 (1996).
- ⁵M. C. Cha, M. P. A. Fisher, S. M. Girvin *et al.*, *Phys. Rev. B* **44**, 6883 (1991); M. P. A. Fisher and G. Grinstein, *Phys. Rev. Lett.* **60**, 208 (1988); M. P. A. Fisher, P. B. Weichman, G. Grinstein, and D. S. Fisher, *Phys. Rev. B* **40**, 546 (1989).
- ⁶W. Krauth, N. Trivedi, and D. Ceperley, *Phys. Rev. Lett.* **67**, 2703 (1991); W. Krauth and N. Trivedi, *Europhys. Lett.* **14**, 627 (1991).
- ⁷C. Bruder, R. Fazio, G. Schön *et al.*, *Phys. Scr.* **T42**, 159 (1992).
- ⁸A. I. Belousov, S. A. Verzakov, and Yu. E. Lozovik, *Zh. Éksp. Teor. Fiz.* **112** (1997), (in press) [*JETP* **85** (1997)].
- ⁹A. L. Dobryakov, V. S. Letokhov, Yu. E. Lozovik *et al.*, *Appl. Phys. A* **54**, 100 (1992).
- ¹⁰S. G. Akopov and Yu. E. Lozovik, *J. Phys. C* **15**, 4403 (1982).
- ¹¹P. Carruthers and M. M. Nieto, *Rev. Mod. Phys.* **40**, 411 (1968); R. Lynch, *Phys. Rep.* **256**, 367 (1995).
- ¹²W. H. Louisell, *Phys. Lett.* **7**, 60 (1963); L. Susskind and J. Glogower, *Physica* **1**, 49 (1964).
- ¹³A. Blaer and J. Han, *Phys. Rev. A* **46**, 3225 (1992).
- ¹⁴P. Minnhagen, *Rev. Mod. Phys.* **59**, 1001 (1987).
- ¹⁵Yu. E. Lozovik and S. A. Verzakov, *Phys. Lett. A* (to be published).
- ¹⁶S. L. Sondhi, S. M. Girvin *et al.*, *Rev. Mod. Phys.* **69**, 315 (1997).
- ¹⁷A. I. Belousov and Yu. E. Lozovik, *Fiz. Tverd. Tela (St. Petersburg)* **39**, 1513 (1997) [*Phys. Solid State* **39**, 1345 (1997)].

Translated by M. E. Alferieff

Phase transition in liquid ^3He in an aerogel at zero temperature

V. P. Mineev

L. D. Landau Institute of Theoretical Physics, Russian Academy of Sciences, 117940 Moscow, Russia

(Submitted 21 October 1997)

Pis'ma Zh. Éksp. Teor. Fiz. **66**, No. 10, 655–660 (25 November 1997)

An expansion of the thermodynamic potential in powers of the order parameter of the superfluid phase transition is found for liquid ^3He in an aerogel at $T=0$. The discontinuity in the compressibility (sound velocity), which is the analog of the discontinuity in the specific heat for second-order temperature phase transitions, is calculated. The magnitude of the critical quantum fluctuations (zero-point vibrations) of the order parameter is estimated. © 1997 American Institute of Physics. [S0021-3640(97)00622-1]

PACS numbers: 67.57.Bc, 64.70.Ja

Aerogels are three-dimensional networks of randomly arranged filaments and plates (20–30 Å thick) of SiO_2 , with an average spacing of several hundred angstroms. The volume of the network material equals about 2% of the volume of space which it occupies, the rest of the space being occupied with liquid helium. It has been established by torsional vibration¹ and nuclear magnetic resonance^{2,3} methods that the superfluid transition temperature and the density of the superfluid component of ^3He in aerogel are appreciably lower than in an ordinary vessel. These effects are associated with the scattering of quasiparticles by the surface, which suppresses the Cooper pairing in the p state⁴ which occurs in superfluid phases of ^3He . The depairing effect of the surface is manifested because the superfluid coherence length (200–800 Å, depending on the pressure) is comparable to the mean free path of the excitations, i.e., to the average pore size in the aerogel.

In contrast to ^3He in a free geometry, where at $T=0$ the ^3He is in a superfluid state at all pressures from zero up to the crystallization pressure ($P_m \approx 35$ atm), in some aerogel samples the influence of the surface is so strong that at low pressures a superfluid phase transition does not occur at all, and the liquid helium remains in the normal state right down to absolute zero temperature. The superfluidity of helium in aerogel arises only at pressures above a critical value (about 6.5 atm in the experiments performed by a group at Cornell University;^{5,6} see Fig. 1). Therefore at $T=0$ a continuous phase transition — a change in the ground state of the liquid — occurs with changing density in ^3He in an aerogel at $T=0$. The theoretical description of this transition is the subject of the present letter.

In what follows we find an expansion of the thermodynamic potential in powers of the order parameter and calculate the discontinuity of the compressibility (sound veloc-

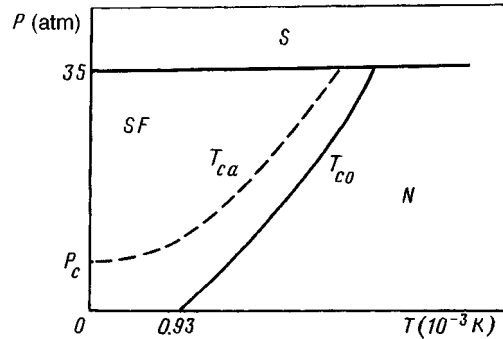


FIG. 1. Phase diagram of ${}^3\text{He}$. S , N , SF — regions occupied by solid, normal liquid, and superfluid helium, respectively. T_{c0} (solid line) and T_{ca} (dashed line) — lines of the superfluid phase transition of helium in a free geometry and in aerogel.

ity), which is the analog of the discontinuity of the specific heat for second-order temperature-induced phase transitions. It is shown that the magnitude of the discontinuity in the sound velocity $\Delta c_{p=P_c}$ at the phase transition in helium in an aerogel is expressed in terms of the derivative of the critical temperature $(\partial T_c / \partial P)_{p=P_c}$ at the phase transition of helium in the free geometry.

The phase transition at $T=0$ in itself is not a more quantum-mechanical phenomenon than is the ordinary phase transition to the superfluid state at finite temperature. Both transitions are due to a rearrangement of the ground state of the liquid as a result of Cooper pairing, which is destroyed in one case by the breakdown of coherence as a result of the thermal motion of the quasiparticles and in the other case by the scattering of the quasiparticles by the surface. A substantial difference of the phase transition at $T=0$ is, however, that in this case the critical fluctuations (zero-point vibrations of the order parameter) have a quantum and not thermal origin. For this reason, the analytical dependences of the fluctuation corrections on the parameter $(P_c - P)/P$ characterizing the proximity to the transition are different from the corresponding functions of $(T - T_c)/T_c$ at a phase transition at finite temperature.

At low pressures the superfluid phase transition of ${}^3\text{He}$ is described well in the weak-coupling approximation. We shall take account of the effect of the aerogel surface in a very simple model of isotropic Born scattering by impurities uniformly distributed over the volume of the liquid. The problem of the effect of the impurities on the superfluid state with p pairing is discussed in Refs. 4 and 7 under the indicated assumptions. It has been shown in a preprint⁷ that, just as in pure ${}^3\text{He}$, in the presence of impurities the B phase with the order parameter

$$d_\alpha(\mathbf{k}) = \Delta(T) R_{\alpha i} \hat{k}_i e^{i\varphi} \quad (1)$$

is energetically favored in the weak-coupling approximation. Here $\Delta(T)$ is the modulus of the order parameter, $R_{\alpha i}$ is the matrix of three-dimensional rotations, and $e^{i\varphi}$ is a phase factor. This result will be used not for solving the general problem of p pairing in liquid helium with impurities at $T=0$ but rather for studying the phase transition from a normal

Fermi liquid to a B phase, i.e., we shall find the expansion of the thermodynamic potential in powers of the modulus $\Delta(T)$ of the order parameter. According to Ref. 4, the equation for determining Δ is

$$1 = \pi N_0 g \sum_{\omega_n} \frac{1}{\sqrt{\tilde{\omega}_n^2 + \Delta^2}}, \quad (2)$$

where N_0 is the density of states, g is the interaction constant, and the quantity $\tilde{\omega}_n$ must be found from the equation

$$\tilde{\omega}_n = \omega_n + \frac{\tilde{\omega}_n}{2\tau\sqrt{\tilde{\omega}_n^2 + \Delta^2}}. \quad (3)$$

Here $\omega_0 = \pi T(2n + 1)$ is the Matsubara frequency and τ is the impurity scattering time (we recall that we are working in the Born approximation taking only s scattering into account). Expanding expression (3) in powers of $\Delta/(\omega_n + \text{sign}\omega_n/2\tau)$, substituting the result into Eq. (2), and once again expanding to second order in Δ , we arrive, in the limit $T \ll 1/4\pi\tau$, at the expression

$$\ln \frac{T_{c0}}{T} = \psi\left(\frac{1}{2} + \frac{1}{4\pi\tau T}\right) - \psi\left(\frac{1}{2}\right) + \frac{\tau^2 \Delta^2}{3}, \quad (4)$$

which, if one neglects the last term, is identical to the equation found in Ref. 4 for the critical temperature. Here $\psi(x)$ is the logarithmic derivative of the Euler gamma function, and $T_{c0} = T_{c0}(P)$ is the superfluid transition temperature in pure helium. For each pressure P one can use Eq. (4) to establish the critical impurity density (mean free time) at which the superfluid transition temperature becomes zero:

$$\tau = \frac{\pi}{\gamma} T_{c0}(P). \quad (5)$$

Here $\ln \gamma = C \approx 0.577$ is the Euler constant.

The critical temperature in pure helium increases with pressure. Let the impurity density be such that the superfluid transition temperature is finite at pressures above some critical value P_c and vanishes at the point $P = P_c$, where the equality (5) is satisfied. Then in the limit $T \rightarrow 0$, we subtract Eq. (4) for $P > P_c$, where $\Delta \neq 0$, from Eq. (4) at the point $P = P_c$, where $\Delta = 0$; this gives

$$\ln \frac{T_{c0}(P)}{T_{c0}(P_c)} = \frac{\tau^2 \Delta^2}{3}. \quad (6)$$

Thus, the modulus of the order parameter in the superfluid phase at $T=0$ near the transition ($P \geq P_c$) is

$$\Delta^2 = \frac{3}{\tau^2} \left. \frac{\partial \ln T_{c0}(P)}{\partial P} \right|_{P=P_c} (P - P_c). \quad (7)$$

Following the standard procedure (see Ref. 8), we reconstruct from this expression the expansion of the thermodynamic potential in powers of the order parameter at zero temperature:

$$\Phi_s - \Phi_N = VN_0 \left(\frac{\partial \ln T_{c0}(P)}{\partial P} \Big|_{P=P_c} (P_c - P) \Delta^2 + \frac{\tau^2}{6} \Delta^4 \right). \quad (8)$$

Here V is the volume of helium. A similar expansion of the thermodynamic potential at zero temperature ($T \ll 1/\tau$) holds in type-II superconductors near the upper critical field ($H \leq H_{c2}$).⁹

Minimizing expression (8) with respect to Δ yields Eq. (7), so that the equilibrium value of $\Phi_s - \Phi_N$ is

$$\Phi_s - \Phi_N = -\frac{3}{2} VN_0 \frac{\pi^2}{\gamma^2} \left(\frac{\partial T_{c0}}{\partial P} \Big|_{P=P_c} \right)^2 (P - P_c)^2. \quad (9)$$

Differentiating expression (9), we find the discontinuity in the specific compressibility

$$\frac{1}{V} \frac{\partial^2 (\Phi_s - \Phi_N)}{\partial P^2} = -\frac{3\pi^2}{\gamma^2} N_0 \left(\frac{\partial T_{c0}(P)}{\partial P} \Big|_{P=P_c} \right)^2, \quad (10)$$

which can formally be rewritten as a discontinuity in the sound velocity

$$\frac{\Delta c}{c} = \frac{c_s - c_N}{c_N} = \frac{3}{2} \frac{\pi^2}{\gamma^2} N_0 \rho c_N^2 \left(\frac{\partial T_{c0}(P)}{\partial P} \Big|_{P=P_c} \right)^2. \quad (11)$$

Here ρ is the density of the liquid. Therefore the discontinuity in the sound velocity at the superfluid phase transition at $T=0$ in helium in an aerogel can be expressed in terms of the pressure derivative of the critical temperature in pure helium in a free geometry. Using the data presented in the review by Wheatley,¹⁰ we obtain the estimate $\Delta c/c \sim 10^{-5}$. Here it should be noted that the propagation of ordinary hydrodynamic sound in helium in an aerogel is impossible. Equation (11) is an estimate of the magnitude of the discontinuity in the velocity of high-frequency sound.

According to the theory of second-order phase transitions¹¹, the result (10), obtained in the self-consistent field approximation, must be compared with the fluctuation contribution arising as a result of zero-point vibrations of the order parameter at $T=0$. The problem of spatially uniform fluctuations in superfluid ^3He in a bounded geometry is solved in Ref. 12. We must solve the problem of spatially nonuniform fluctuations of the order parameter in the normal phase near the transition point $P = P_c$. In view of the fact that in the general case the order parameter in a superfluid liquid with p pairing is given by a matrix $A_{\alpha i}$ (a 3×3 matrix depending on 18 real variables), the quantitative description of quantum fluctuations is very complicated, even in a model with a uniform distribution of randomly located impurities. There are also specific features due to fluctuations of the spontaneous orbital (and spin) angular momentum of the liquid, which give rise to terms linear in the time derivative in the kinetic energy of the liquid.¹³ Here we confine ourselves to estimating the fluctuation effects, making the assumption that only the complex amplitude of the order parameter $A = \Delta e^{i\varphi}$ fluctuates (see Eq. (1)).

The term in the fluctuation energy quadratic in the order parameter has the form

$$F = N_0 \int dV \left\{ a \tau^2 \left| \frac{\partial A}{\partial t} \right|^2 + \alpha |A|^2 + b v_F^2 \tau^2 |\nabla A|^2 \right\}. \quad (12)$$

Here a and b are numerical constants

$$\alpha = \alpha_0 (P_c - P) = \left. \frac{\partial \ln T_{c0}(P)}{\partial P} \right|_{P=P_c} (P_c - P),$$

and v_F is the Fermi velocity. The gradient terms in Eq. (12) can be easily obtained, performing the integration in the limit $T \rightarrow 0$, from the formulas presented in Ref. 7 for the coefficients in the gradient energy. Switching to the Fourier representation

$$A(\mathbf{r}, t) = \sum_k e^{i\mathbf{k} \cdot \mathbf{r}} A_k(t),$$

we can write the energy (12) as a sum of the Hamiltonians of harmonic oscillators

$$H = \frac{1}{2} \sum_k (P_k^2 + \omega_k^2 Q_k^2), \quad (13)$$

where

$$P_k = -i \omega_k \sqrt{N_0 a \tau^2} (A_k - A_k^*), \quad Q_k = \sqrt{N_0 a \tau^2} (A_k + A_k^*), \quad \omega_k = \left(\frac{\alpha + b v_F^2 \tau^2 k^2}{a \tau^2} \right)^{1/2}.$$

The energy of the zero-point vibrations of the order parameter is

$$E_0 = \frac{1}{2} \sum_k \omega_k \quad (14)$$

and the corresponding quantum contribution to the specific compressibility of the system is

$$\frac{1}{V} \frac{\partial^2 E_0}{\partial P^2} = - \frac{\alpha_0^2}{4 a \tau (2 \pi)^3} \int \frac{d^3 k}{(\alpha + b v_F^2 \tau^2 k^2)^{3/2}}. \quad (15)$$

In contrast to the fluctuation correction to the specific heat, the quantum correction to the specific compressibility diverges logarithmically for large values of k , which corresponds to power-law (and not exponential!) behavior of the correlation function $\langle A(0) A^*(R) \rangle$. Cutting off the integral in Eq. (15) at k_F , we obtain to logarithmic accuracy

$$\frac{1}{V} \frac{\partial^2 E_0}{\partial P^2} = - \frac{\alpha_0^2}{2 (2 \pi)^2 a b^{3/2} v_F^3 \tau^4} \ln \frac{\epsilon_F \tau}{\alpha_0 (P_c - P)}. \quad (16)$$

Here ϵ_F is the Fermi energy. Comparing this quantity to the discontinuity of the compressibility obtained in the self-consistent field theory (10) shows that the quantum correction is small at all pressures for which

$$\left. \frac{\partial \ln T_c(P)}{\partial P} \right|_{P=P_c} (P_c - P) > \left(\frac{\epsilon_F}{T_{c0}} \right)^2 \exp \left(- \left(\frac{\epsilon_F}{T_{c0}} \right)^2 \right). \quad (17)$$

In this expression we deliberately dropped all numerical coefficients in order to underscore the parametric smallness of the right-hand side.

In summary, the compressibility of liquid ^3He at a phase transition at $T=0$ in aerogel has a discontinuity whose magnitude can be expressed in terms of a derivative of the critical temperature of helium in the free geometry. This property apparently holds only in the present model of isotropically scattering impurities. To develop a more realistic theory of superfluid ^3He in aerogels it is necessary to take into account the anisotropy of quasiparticle scattering by the aerogel surface. The resulting quantum corrections to the magnitude of the discontinuity are significant only in a negligibly narrow neighborhood of the phase transition.

In closing, it is my pleasant duty to thank Professor J. Parpia, from whose report at the P. L. Kapitza Institute I learned of the phase transition in ^3He in aerogel at $T=0$, and Yu. S. Barash for calling to my attention the question of estimating the quantum fluctuation corrections. I am also appreciative of the active interest shown by V. V. Lebedev, D. Fel'dman, and A. F. Andreev in this work. This work was supported by the Ministry of Science of the Russian Federation (the program ‘‘Statistical Physics’’), the Russian Fund for Fundamental Research (Grant 96-0216041), and the INTAS program (Grant 96-0610).

¹J. V. Porto and J. M. Parpia, Phys. Rev. Lett. **74**, 4667 (1995).

²D. T. Sprague, T. M. Haard, J. B. Kycia *et al.*, Phys. Rev. Lett. **75**, 661 (1995).

³D. T. Sprague, T. M. Haard, J. B. Kycia *et al.*, Phys. Rev. Lett. **77**, 4568 (1996).

⁴A. I. Larkin, JETP Lett. **2**, 130 (1965).

⁵K. Matsumoto, J. V. Porto, L. Pollack *et al.*, Phys. Rev. Lett. **79**, 253 (1997).

⁶J. V. Porto, A. Golov, K. Matsumoto *et al.*, preprint, Cornell University, August 27, 1997.

⁷E. V. Thuneberg, S. K. Yip, M. Fogelström, and J. A. Sauls, Preprint <http://xxx.lanl.gov/abs/cond-mat/9601148>.

⁸E. M. Lifshitz and L. P. Pitaevskiĭ, *Statistical Physics*, Pergamon Press, Oxford, 1950 [Russian original, Nauka, Moscow, 1978, part 2].

⁹M. G. Vavilov and V. P. Mineev, Zh. Éksp. Teor. Fiz. **112**, 1873 (1997) [JETP **85** (1997)] (in press).

¹⁰J. C. Wheatley, Rev. Mod. Phys. **47**, 415 (1975).

¹¹L. D. Landau and E. M. Lifshitz, 3rd ed. *Statistical Physics*, Pergamon Press, Oxford, 1980 [Russian original, Nauka, Moscow, 1976, part 1].

¹²K. B. Efetov and M. M. Salomaa, J. Low Temp. Phys. **42**, 35 (1981).

¹³I. A. Fomin, Phys. Lett. A **66**, 47 (1978).

Translated by M. E. Alferieff

Formation of amorphous carbon on melting of microcrystalline graphite by picosecond laser pulses

M. B. Agranat,^{a)} S. I. Ashitkov, A. V. Kirillin, A. V. Kostanovskii,
and V. E. Fortov

Scientific-Research Center of Thermal Physics of Pulsed Effects, Joint Institute of High Temperatures, Russian Academy of Sciences, 127412 Moscow, Russia

S. I. Anisimov

L. D. Landau Institute of Theoretical Physics, Russian Academy of Sciences, 142432 Chernogolovka, Moscow Region, Russia

P. S. Kondratenko

Institute of the Problems of Safe Development of Atomic Energy, Russian Academy of Sciences, 113191 Moscow, Russia

(Submitted 23 October 1997)

Pis'ma Zh. Éksp. Teor. Fiz. **66**, No. 10, 661–665 (25 November 1997)

Observations of microcrystalline graphite subjected to picosecond laser pulses reveal the formation of a liquid phase with a subsequent transition to a uniform amorphous state of a surface layer upon solidification. This phenomenon is observed on a definite type of graphite and with the radiation incident on a plane parallel to the sixfold symmetry axis, and only for certain parameters of the laser pulse. A structural analysis of the amorphous phase is performed by electron microscopy and Raman scattering spectroscopy. A periodic structure with a period of the order of the wavelength of the heating pulse is formed in the heating region. The “rulings” of this periodic structure are oriented in the direction of polarization of the heating pulse. A study of the reflection kinetics of the probe laser pulse showed that the characteristic existence time of the liquid phase and of the solidification process is $\sim 10^{-10}$ s.
© 1997 American Institute of Physics. [S0021-3640(97)00722-6]

PACS numbers: 81.05.Gc, 81.05.Tp, 64.70.Dv

There have now been a considerable number of studies, which are not completely in accord with one another (see, for example, Refs. 1–3), devoted to the formation of a liquid phase of carbon under the action of femto- and picosecond laser pulses on graphite. The differences in the approaches to this problem stem from the difficulty of coming up with an unambiguous interpretation of the results, from the imperfection of the methods used to detect liquid carbon, and from the fact that the surface crystallizes on cooling — only traces of amorphous carbon are observed, but they can also be present in the initial sample. In the review by Reitze *et al.*² it is asserted, for example, that the observation of liquid carbon at atmospheric pressure is possible only for subpicosecond times, when hydrodynamic excitation of the heated layer and expansion of the vaporized matter do not occur.

We report in this letter the observation of a liquid carbon phase, formed by the action of picosecond laser pulses on a definite type of carbon under certain experimental conditions, and the formation of a completely amorphous surface layer of carbon upon solidification of the melt.

The experimental investigations were performed using a laser system based on multicascade stimulated Brillouin and stimulated Raman compression of the initial nanosecond pulse of a Nd:YAG laser which generates simultaneously several pulses of different duration in the femto- and picosecond time ranges with a repetition frequency of up to 10 Hz. The parameters were monitored using a measurement system that included pulse-energy photosensors, an electron-optical camera (EOC) with ~ 3 ps resolution, an autocorrelator with ~ 50 fs resolution, and a system for measuring the spectrum of a pulse. All measurements, including diagnostics, were fed into a multichannel digital data reading and processing unit consisting of several highly sensitive digital CCD — video cameras and analog-signal inputs, an data reading synchronization unit, a unit for controlling the laser system, and a computer that made it possible to control the system according to a prescribed program and to extract and process simultaneously data from the output of the EOC, oscillograph, autocorrelator, energy sensors, photodetectors, and spectral devices.

Transmission electron microscopy, x-ray diffractometry, and Raman scattering spectroscopy investigations of the starting sample showed that the initial material consists of microcrystalline graphite with 10–30 nm grains. The graphite sample was prepared in the form of a tablet (Fig. 1a), whose flat surface (called “surface” below) was perpendicular to the *C* symmetry axis. Accordingly, the lateral face of the tablet (“end” below) is parallel to the symmetry axis. The diffraction pattern for the surface of the sample is reminiscent of the diffraction pattern in the case when the crystallites have a preferred, predominant orientation. The graphite layers are parallel to one another but their spacing is not fixed. A clearly expressed texture is observed, i.e., the microcrystallites are slightly disoriented with respect to one another. It can be concluded from the results of these investigations that the properties of this sample (specifically, the thermal conductivity) are strongly anisotropic.

The heating laser pulse was focused into a spot ~ 200 μm in diameter on the end and surface of the graphite (Fig. 1a). In addition, on the end, the plane of polarization of the heating pulse in the spot 1 made an angle of 45° with respect to the direction of polarization in the spot 2. Under the repeated action of the laser pulses with a repetition frequency of 10 Hz, a strongly reflecting microregion (the reflectance is three to four times higher than the initial reflectance) arises at the center of the focal spot on the end and grows to the size of the focal spot. The reflectance increases very little in the plane of the “surface.” Figure 1b displays an image (obtained with a CCD camera) of the heating region on the end under the action of ~ 150 laser pulses. Electron microscopy showed that in all spots there is a periodic surface relief with period ~ 0.6 μm in the spots on the end and with a period of ~ 1 μm in the spots on the surface. The “rulings” in spot 2 are oriented parallel to the graphite layers, and in spot 1 they are at an angle of 45° . The structure on the surface of the sample is not as sharp as that on the end.

The Raman spectra (Fig. 2) showed that for the crater on the surface of the sample the presence of an amorphous phase of carbon is identified both at the center and periph-

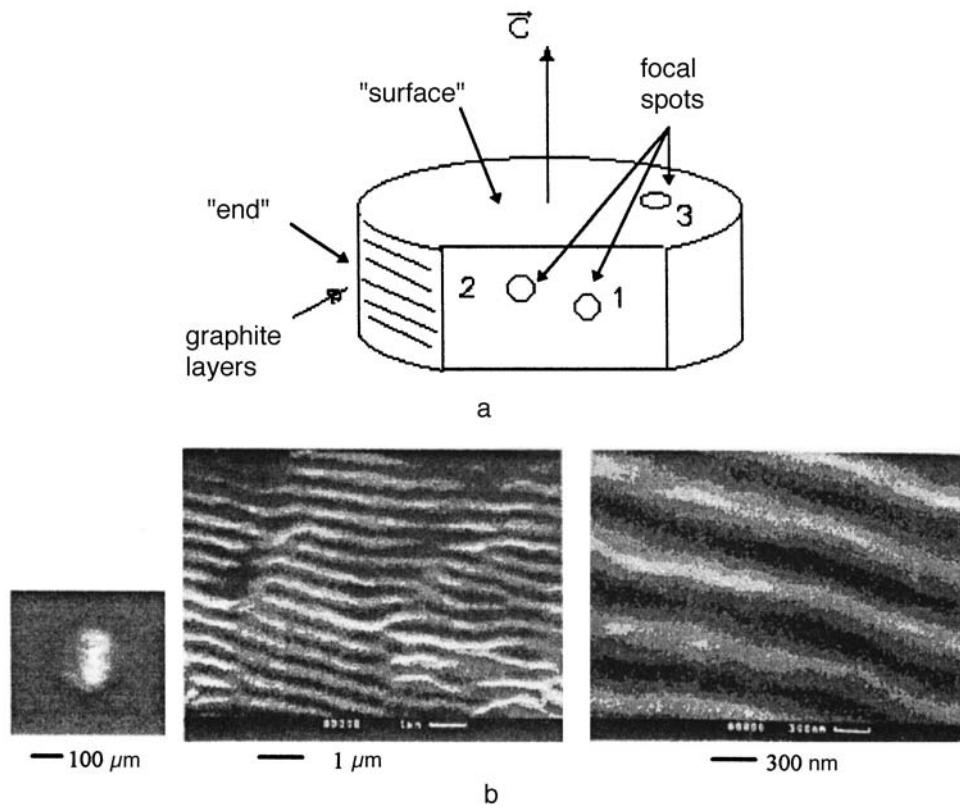


FIG. 1. Formation of periodic structure: a) Arrangement of the focal spots of the heating pulse on the graphite sample; b) form of the periodic structure under different magnifications.

ery of the crater. The amorphous phase fraction is higher at the center of the crater. Reflections corresponding to a microcrystalline phase of graphite are observed at these same points simultaneously with an amorphous phase. At the same time, Raman mea-

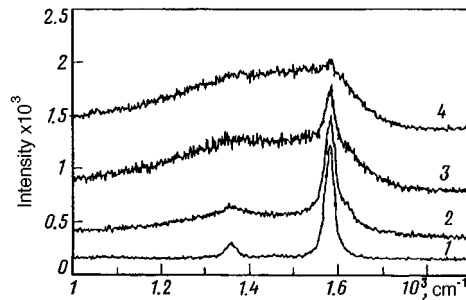


FIG. 2. Raman scattering spectra: 1 — Initial sample; 2 — spot 3 ("surface"), periphery; 3 — spot 3, center; 4 — spots 1, 2 ("end"), periphery, center.

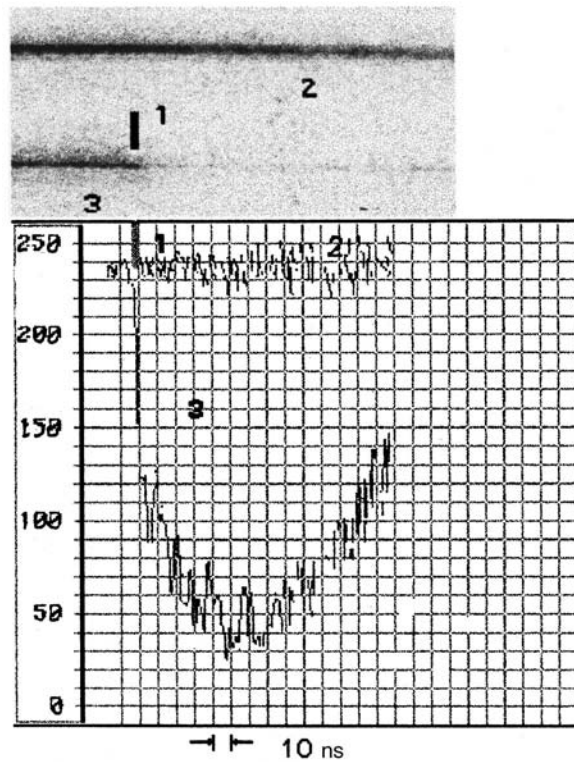


FIG. 3. Characteristic photochronograms of the p component of the probe laser pulse (2) and the s component of the reflected probe pulse (3), 1 — heating laser pulse.

measurements in both spots on the end of the sample show the presence of only an amorphous phase of carbon, without any traces of microcrystalline graphite.

The reflection dynamics was studied with an “Agat” electroon-optical camera (EOC) with 3 ps resolution. A ~ 500 ps probe laser pulse, having a wavelength of 530 nm and polarized in the plane of incidence (p wave), was focused into a $50 \mu\text{m}$ spot. The angle of incidence did not exceed 15° . The coincidence of the spots of the heating and probe pulses was monitored with a CCD camera through a microscope with a magnification of $70\times$. The reflected probe pulse transmitted by a crossed analyzer (s wave), the incident probe pulse (p wave), and the heating pulse (serving as a time reference) were directed onto the input slit of the EOC. Measurements on the end were performed in a crater produced by the repeated action of the laser pulses, i.e., in the presence of an amorphous phase and a periodic surface structure. Figure 3 displays the characteristic photochronograms of the probe pulse (including processing with allowance for the temporal shape of the laser pulse). These photochronograms show that upon arrival of the heating pulse, the intensity of the s component of the reflected probe pulse drops sharply (with characteristic time < 3 ps), and then it starts to grow after 100–150 ps have elapsed. (To follow the temporal shape of the reflected pulse in the subnanosecond and

longer ranges, the probe pulse duration must be increased; this is a subject of further investigations).

Thus, the following conclusions can be drawn from an analysis of the results of these investigations. The appearance of periodic surface structures is due to resonance excitation of surface electromagnetic waves.⁴ The study of this phenomenon in graphite is of interest in itself. In our case, the periodic structures play the role of an artificial anisotropy, the presence or vanishing of which can be monitored by means of the partial *p*- to *s*-waveconversion on reflection.⁵ The dependence of the direction of the “rulings” of the periodic structure on the polarization direction of the heating pulse shows that the formation of the structure is not affected by the layered structure of the graphite and most likely occurs in a melt of the heated layer. The measurements of the reflection kinetics suggest the following picture. Under the action of the heating pulse a surface layer of the graphite melts with a characteristic time of less than 3 ps. The shortness of this time attests to the fact that melting occurs by homogeneous nucleation, i.e., it is of a bulk character. The transition to a uniform amorphous state on the end of the sample on solidification of the heated layer can be explained by the fact that as a result of the anisotropy of the thermal conductivity, the layer on the end of the sample cools much more quickly than the layer on the surface.

We owe a debt of gratitude to S. G. Konnikov, Director of the St. Petersburg Joint Research Center, and to the staff at the Center for assisting in the analysis of the structure of the graphite samples.

This work was supported by the Russian Fund for Fundamental Research under Grants 96-02-18494/a and 96-02-18495/a.

^{a)}e-mail: agranat@tiv.phys.msu.su

¹A. M. Malvezzi, N. Bloembergen, and C. Y. Huang, *Phys. Rev. Lett.* **57**, 146 (1986).

²D. H. Reitze, H. Ahn, and M. C. Downer, *Phys. Rev. B* **5**, 2677 (1992).

³X. Y. Wang and M. C. Downer, *Opt. Lett.* **17**, 1450 (1992).

⁴A. M. Bonch-Bruevich, M. N. Libenson, V. S. Makin, and V. V. Trubaev, *Opt. Eng.* **31**, 718 (1992).

⁵M. B. Agranat, S. I. Anisimov, S. I. Ashitkov *et al.*, *Zh. Èksp. Teor. Fiz. [JETP]* (in press).

Translated by M. E. Alferieff

ERRATA

Erratum: Does the Unruh effect exist? [JETP Lett. 65, No. 12, 902–908 (25 June 1997)]

V. A. Belinskiĭ

INFN and ICRA, Rome University “La Sapienza,” 00185 Rome, Italy

B. M. Karnakov, V. D. Mur, and N. B. Narozhnyiĭ

Moscow State Engineering-Physics Institute, 115409 Moscow, Russia

[S0021-3640(97)00822-0]

PACS numbers: 03.70.+k, 04.60.-m, 99.10.+g

On page 905, the second sentence after Eq. (18) should read: “If here the surface $t=0$ is taken as the surface of integration and the fact that the modes $R_\mu=0$ for $z<0$ and are functionally the same as the Fulling modes (3) for $z>0$ is taken into account, then after making the change of variables (8) it might seem that $(R_\mu, \phi)_M = (\Phi_\mu, \phi)_R$.”